

AN ABSTRACT OF THE THESIS OF

Andra L. Shaughnessy for the degree of Master of Science in Nuclear Engineering
presented on April 10, 2012.

Title:Predicting Antineutrino Source Terms from a High Temperature Gas Reactor

Abstract approved: _____

Todd S. Palmer

Since the 1990s, researchers around the world have been creating antineutrino detectors for monitoring power reactors. These detectors have been deployed at light water reactors and are able to determine power levels and burn up throughout a fuel cycle. This technology could allow the IAEA to monitor LWRs remotely and unobtrusively to determine if they are operating using normal parameters. Very soon, the next generation of detector will be deployed at a CANDU reactor for a trial operation.

While physical observation of these detectors is necessary in determining their usefulness, reactor physics simulations have proven to be very accurate in their prediction of detector performance. Since there are many designs still in development, reactor physics simulations are the only way to determine the efficacy of the detector technology. In addition to this, reactor simulations are the best way to evaluate the detector technology to ascertain its usefulness during diversion scenarios.

In this research, antineutrino source terms were calculated for a High Temperature Gas Cooled Reactor core. These source terms were a function of power level and initial enrichment. SCALE6.1, developed by Oak Ridge National Laboratory, was used to calculate the isotopic inventory in the core as a function of depletion.

These fertile and fissile isotopes, along with the fission cross-section and number of antineutrinos emitted per fission, were used to predict the antineutrino source rate for the core. It was found that changing the power yields a linear response from the antineutrino source term. By increasing the power by five percent, the source term also increased by five percent. Substantial changes in the initial enrichment also lead to a detectable change in the antineutrino source term.

©Copyright by Andra L. Shaughnessy

April 10, 2012

All Rights Reserved

Predicting Antineutrino Source Terms from a High Temperature Gas Reactor

by

Andra L. Shaughnessy

A THESIS

submitted to

Oregon State University

in partial fulfillment of
the requirements for the
degree of

Master of Science

Presented April 10, 2012
Commencement June 2012

Master of Science thesis of Andra L. Shaughnessy presented on April 10, 2012.

APPROVED:

Major Professor, representing Nuclear Engineering

Head of the Department of Nuclear Engineering and Radiation Health Physics

Dean of the Graduate School

I understand that my thesis will become part of the permanent collection of Oregon State University libraries. My signature below authorizes release of my thesis to any reader upon request.

Andra L. Shaughnessy, Author

ACKNOWLEDGEMENTS

There have been so many people who have helped me with this journey that I don't even know where to start. I guess the top is always the best place.

Thank you God for giving me the strength and ability to complete this task even when I wanted to do nothing more than quit. To my parents, Gene and Jana: You've been there through the good and the bad and never doubted that I would accomplish this feat even when I questioned myself. I could not ask for more. I love you both so much. Kayla, Kalli and Elle: Thank you for helping me keep everything in perspective and reminding me that there is more to life than school. You three are the best and I love you all so much. Michael: Thanks for the distractions that kept me sane. To my grandparents: Thank you for believing in me and praying for me. I couldn't have done it without your support. To my extended family and friends: Thank you for letting me ramble on about my work and pretending to be interested in what I was saying. You guys are a great ego boost. Mrs. Redfern: I doubt you'll ever know the impact you have on your students. You gave me the initial push down this roller coaster and I'll forever be grateful for it. Dr. S, Dr. K, Dr. L and all my other professors: Thanks for explaining things to me endlessly until I finally understood. Topher and Elan: Thanks for your patience and your help. I could always count on you guys when I was stuck. Jill and Brian: I would not have made it through all those classes without your hours of explanation. Thanks so much.

Dr. Palmer: Thank you for your endless patience and your willingness to work around whatever was going on in my life. I was very lucky the day you called and offered me an assistantship under you. I wish you the very best in your new career.

TABLE OF CONTENTS

	<u>Page</u>
1 Introduction	1
2 Literature Review	3
2.1 Research around the world	3
2.1.1 Russia	3
2.1.2 France	3
2.1.3 Brazil	5
2.1.4 Japan	5
2.1.5 United States	5
2.1.6 SONGS1	6
2.1.7 Non-flammable Detectors	8
2.2 High Temperature Gas-Cooled Reactor	11
2.2.1 Peach Bottom Reactor	11
2.2.2 Fort St. Vrain	13
2.2.3 GT-MHR	14
2.2.4 VHTR	14
2.3 Research Objectives	18
3 Materials and Methods	19
3.1 TRISO Fuel	19
3.2 NEWT	22
3.3 Core Simulations	26
3.4 Antineutrino Detector	28
3.5 Verification of Results	29
4 Results	32
4.1 Changing Enrichment	33

TABLE OF CONTENTS (Continued)

	<u>Page</u>
4.2 Changing Power Levels	35
4.3 Antineutrino Detector	36
5 Conclusions	41
5.1 Discussion of Results	41
5.2 Future Work	42
Bibliography	43
Appendices	46
A Sample SCALE code for HTGR	46
B Power Peaking by Fuel Rod	54
C Illustration of NEWT	56

LIST OF FIGURES

Figure	Page	
1	France has been conducting research on the Double Chooz detector in hopes that it might be a viable nonproliferation tool.	4
2	SONGS1 is the first antineutrino detector prototype created within the United States. The research was done by LLNL and Sandia [6].	7
3	The detector is placed in the tendon gallery of the reactor so that it is out of the way of day to day operations [6].	8
4	After seeing some of the downsides of the first detector, LLNL and Sandia came up with a second prototype, SONGS2[6].	9
5	A diagram of a general pebble bed reactor[13].	12
6	The core of the VHTR still uses the annular design of the GT-MHR [19].	15
7	Like the GT-MHR, the VHTR reactor is designed to leave as small of a footprint as possible [19].	17
8	A TRISO kernel is made up of different layers which work together to combat the extreme temperatures[22].	20
9	TRISO fuel particles are tiny. They are first compressed together to form a compact and then the compacts are arranged to create a fuel assembly[23].	21
10	The Amoeba Effect occurs when the fuel kernel is thermally driven toward the hot side of the microsphere[20].	22
11	Comparison of burnup calculations found by use of Serpent and TRITON-NEWT for a prismatic block without burnable poison.[25].	23
12	A representative computational cell to use as a visual when deducing how NEWT solves the transport equation[24].	25
13	The power distribution by ring in the core[28].	27
14	A single fuel compact.	28
15	a. Spatial mesh grid for original parameters. b. Spatial mesh grid for new parameters to test for convergence.	31
16	Antineutrino source term by isotope for normal reactor operating parameters.	32
17	Antineutrino rate of U-238 when changing the enrichment of the fuel.	34
18	Antineutrino rate of U-235 when changing the enrichment of the fuel.	35
19	Antineutrino rate of Pu when changing the enrichment of the fuel. .	36
20	Antineutrino rate of U-238 when changing the power density of the reactor.	37
21	Antineutrino rate of U-238 when changing the power density of the reactor.	38
22	Antineutrino rate of Pu when changing the power density of the reactor.	39

LIST OF FIGURES (Continued)

<u>Figure</u>		<u>Page</u>
23	Total number of antineutrinos for each simulation.	40
24	Used to determine power density in the 6th ring of the core[28]. . .	54
25	Used to determine power density in the 7th ring of the core.	55
26	Used to determine power density in the 8th ring of the core.	55
27	An illustration of how NEWT solves a transport problem[24].	56

LIST OF TABLES

<u>Table</u>		<u>Page</u>
1	Checking convergence of different simulations by changing different parameters.	30
2	Percent difference in antineutrino source term with changes in enrichments.	33
3	Percent difference in antineutrino source term with changes in power levels.	38
4	Detector Antineutrino Counts Per Day	39

I'm dedicating this work to Gayle Wayland who passed away May 18, 2010. No one believed in me more or thought that this was more possible than her. She was my anchor and my best friend, truly the best grandmother a girl could ask for. I'll always love you Grandma!!!

Predicting Antineutrino Source Terms from a High Temperature Gas Reactor

1 Introduction

On August 6th, 1945, the United States dropped the first atomic bomb on Hiroshima, Japan followed three days later by another atomic bomb on Nagasaki, Japan. An estimated 225,000 people were killed and countless others were injured or later developed cancer as a direct result of the bombings.

As the number of countries developing nuclear weapons grew, researchers were figuring out new ways to use nuclear technology for electricity generation. It could provide relief to all the countries who were lacking in natural resources needed for generation of process heat such as water and coal. While nuclear reactors can be expensive to build, once they are up and running, they provide cheap electricity so developing countries can improve their standard of living. The only problem is that in order to run a nuclear reactor, one must have fissile material, the same material used to make atomic bombs. In December of 1953, President Dwight D Eisenhower gave his Atoms for Peace speech and this gave way to the birth of the International Atomic Energy Agency (IAEA) in 1957. The IAEA is an international group that oversees the spread of nuclear technology, ensuring that the technology is being used for peaceful purposes and not for nuclear weapons [1]. In 1968, the Treaty on Nonproliferation of Nuclear Weapons was placed into effect. This treaty stated that the signers would use nuclear technology only for energy purposes and not for weaponry. Each of the countries who had nuclear weapons at the time signed it.

The IAEA did its best to keep the number of countries who could develop nuclear weaponry to a minimum but the technology was still discovered by others. Currently seven countries admit to having developed nuclear weapons: the United

States, Russia, the United Kingdom, France, China, India, and Pakistan. South Africa had nuclear weapons at one time but dismantled in a show of supporting peace. Two other countries, Israel and North Korea, have not admitted to having them but it is considered likely that they do. This is even more serious than many people realize because today's nuclear weapons are approximately 1500 times more destructive than the bombs dropped on Japan. The devastation would be even more catastrophic if one of these was detonated in a densely populated area.

The IAEA is responsible for developing a safeguard system to make sure countries are not creating nuclear weapons. This system involves on site inspections performed by the IAEA to ensure that the amount and type of nuclear fuel material is what would be expected for power generation. The problem with these inspections is that it is very easy to hide anything that should not be there. A country involved with creating nuclear weapons can still stockpile plutonium and then place it somewhere other than the reactor and the inspectors will never know. It is a flawed system but until recently there has been no other way of detecting the intentional excessive production of plutonium.

Antineutrino detection is the next nonproliferation tool in the IAEA's arsenal. With antineutrino detectors, it is possible to watch the reactor as it is active and measure its operating power level. This means that if a reactor is being operated to produce quantities of weapon-usable plutonium, the IAEA will know in live time and will be able to send someone in to stop the stockpiling before it can become a serious issue. An antineutrino detector could be the answer to the problem of how to stop other nations from developing nuclear weapons.

2 Literature Review

Research on antineutrino detectors has been going on for quite a while and the United States is not the only country who sees a future in this work. Scientists from across the globe are trying to develop new techniques and detectors that will make sure that nuclear weapons do not spread to more nations, especially hostile ones.

2.1 Research around the world

2.1.1 *Russia*

The idea of using antineutrinos for monitoring reactors was first conceived by Mikaelian [2]. In the 1990's, the Rovno experiment was the first to demonstrate the correlations between the reactor antineutrino flux, thermal power and fuel burnup. Research is still going forward in this area as many of those who worked on the Rovno experiment are still working in this field. Currently a new gadolinium scintillator is being developed that uses a linear alkylbenzene solvent. These researchers are currently proposing building a new detector one cubic meter in volume and installing it at a Russian reactor to gauge the success of the detector for reactor safeguarding.

2.1.2 *France*

France is currently working on two different types of detectors. The first is called the Double Chooz [3] (See Figure 1). This detector is sitting about four hundred meters from the two Chooz reactors and is being used for precise measurement of antineutrinos with nonproliferation goals in mind. This detector will be the newest technology for antineutrino detection and should be able to perform a benchmark

measurement for the antineutrino energy spectrum emitted by a commercial pressurized water reactor (PWR). The French are also hoping that with their new detector they will be able to use the gathered data to create better reactor simulations so that they will be able to predict more accurately the fission rates and energy spectra emitted by fissioning isotopes.

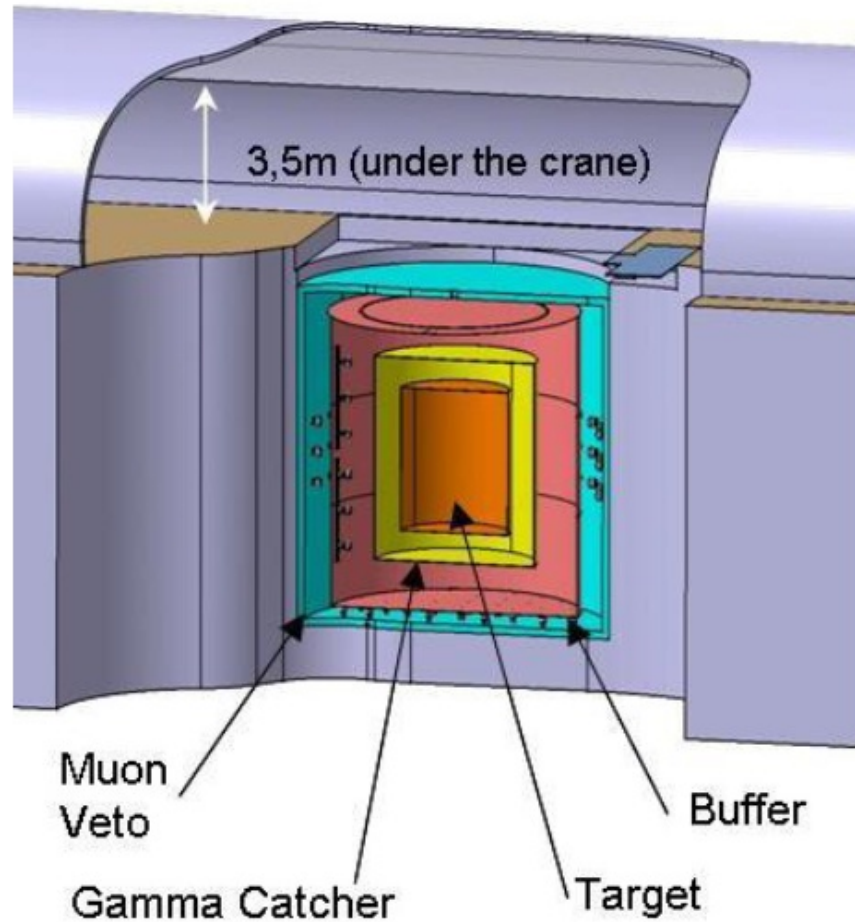


Figure 1: France has been conducting research on the Double Chooz detector in hopes that it might be a viable nonproliferation tool.

Many consider the Double Chooz detector too complex and expensive for widespread use and so the French are also developing Nucifer, a more compact detector with similar technology. The emphasis of Nucifer is to keep a high detec-

tion efficiency of about 55% and good energy resolution. As with Double Chooz, Nucifer will be deployed near a commercial PWR to measure reactor fuel cycle using antineutrino detection.

2.1.3 Brazil

The Angra dos Rios Nuclear Power Plant is currently being prepared for an antineutrino detector deployment [4]. The research being done in Brazil is exciting because a third reactor is being installed with a designed space for a new detector. This detector will be very compact and used for reactor safeguard purposes. At this point, it is still in a trial stage but the results from this experiment could go a long way in determining if installing detectors at the time of reactor installation will be a viable strategy for nonproliferation.

2.1.4 Japan

The KASKA theta-13 experiment involves the development and deployment of a prototype detector at the Joyo fast research reactor [5]. This experiment is noteworthy because the detector is installed near a small research reactor with little overburden. The IAEA has expressed interest in using this technique in this type of environment. Unfortunately, so far the detector has counted a very high background rate and has not identified a single clear reactor antineutrino signal.

2.1.5 United States

While many different countries are making headway on using antineutrino detection as a nonproliferation tool, some of the most promising research has been completed in the United States. Lawrence Livermore National Lab (LLNL) and Sandia National Lab have been working together to create a detector that is both

non-intrusive and highly efficient.

2.1.6 SONGS1

The first prototype created by the US was the SONGS1 detector [6] (See Figure 2). It detects the inverse beta decay reactions by means of a gadolinium-doped proton-rich scintillator. An antineutrino collides with a proton in the scintillator which produces a positron and a neutron (See Eqn 1). Nanoseconds later, the positron is annihilated when it interacts with an electron [7].



The annihilation reaction generates a blue scintillation light. Thirty microseconds after the initial flash, the neutron which has been traveling in the scintillator is captured by a gadolinium nucleus. This produces a second flash of light. A photomultiplier tube detects these two bright pulses and records them as an antineutrino interaction in the detector.

SONGS1 was deployed at the San Onofre Nuclear Generating Station which is a 2,254 megawatt reactor. The detector was installed about ten meters underground at a twenty-five meter distance from the reactor core [8] (See Figure 3). The location was ideal because it did not disrupt the day to day operations of the reactor or its workers. Also, because it was located in the tendon gallery [9], the detector was protected from cosmic rays that could spoof false positives of an antineutrino reaction. One in every 100,000 antineutrinos produced by the reactor passed through the detector. This meant that about 10^{17} antineutrinos passed through the detector each day and that approximately 4,000 collided with a proton. Of these, about 400 result in a detectable signature giving the detector an efficiency of approximately ten percent [10]. The results from the first trial were

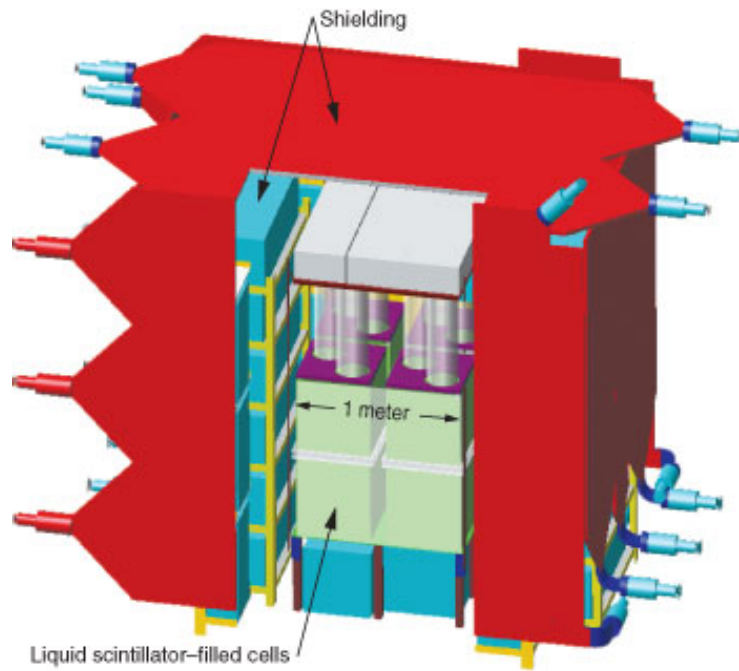


Figure 2: SONGS1 is the first antineutrino detector prototype created within the United States. The research was done by LLNL and Sandia [6].

very promising. The researchers were able to measure the reactor's power level to an accuracy of three percent. In addition to this, they were able to tell within five hours if there had been a SCRAM [11].

While SONGS1 had a very successful initial deployment, there were several drawbacks to the design. For one, the detector was very large and heavy. With shielding, it measured three meters on a side and weighed 25 tons. Secondly, the scintillator was flammable as well as toxic and carcinogenic. This meant that it had to be transported as hazardous material and therefore was not a design that would be easily deployed around the world.

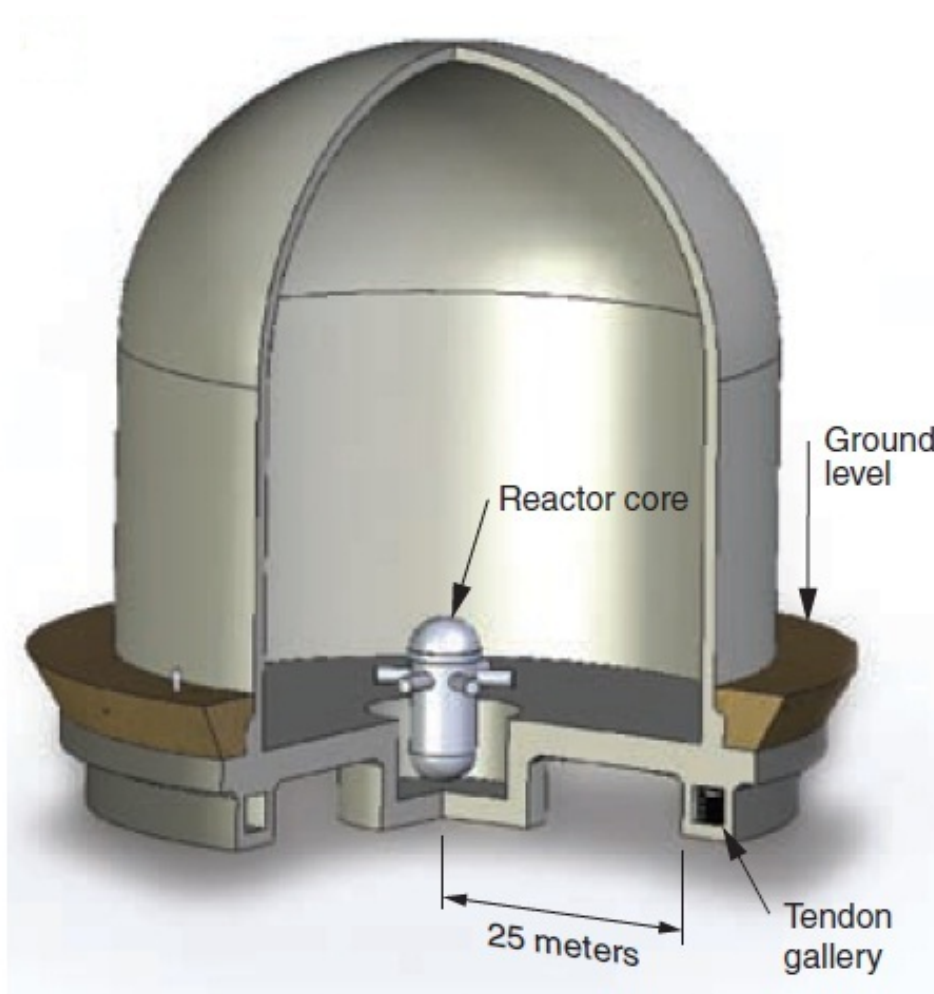


Figure 3: The detector is placed in the tendon gallery of the reactor so that it is out of the way of day to day operations [6].

2.1.7 Non-flammable Detectors

Even though SONGS1 was very successful, its drawbacks were enough to make the researchers look into a different detector that would be smaller and less dangerous. The SONGS2 detector (See Figure 4) used a plastic scintillator [11] instead of a liquid. To avoid the gadolinium degrading the plastic's transparency, the gadolinium was mixed into a paint and spread over two-centimeter-thick plastic sheets to form a one-millimeter-thick layer. These painted plastic sheets were then alternated

with pieces of the plastic scintillator. This new design allowed the antineutrino to collide with a proton in the plastic scintillator which produced a positron. The creation of the positron induced a flash of light, and the resulting neutron travels through the plastic until it is captured by the gadolinium paint. As before, the gamma rays created by the neutron capture produce another flash of light. While this second detector is no longer flammable, it still requires special shielding to keep out the cosmic rays and therefore is still bulky and causes a large “footprint” at the reactor.

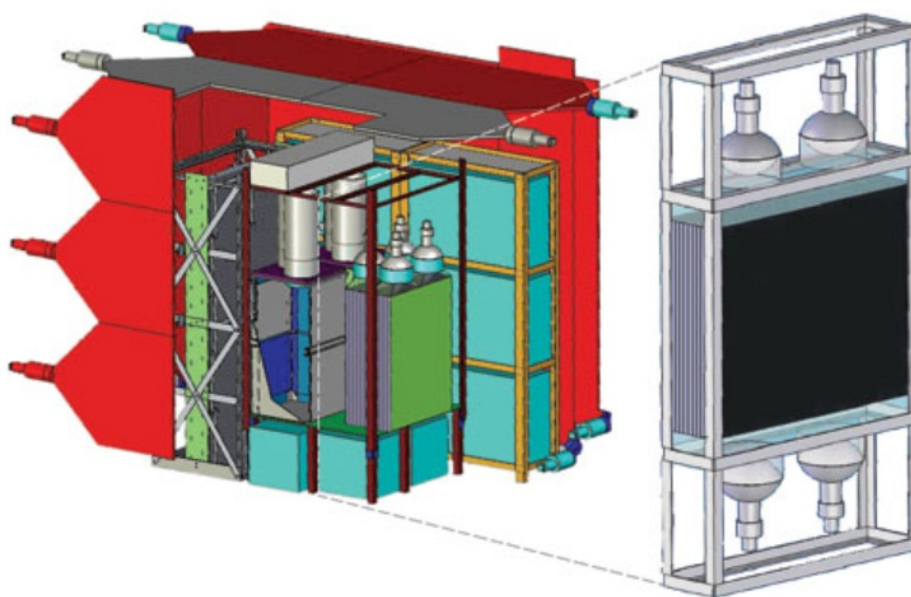


Figure 4: After seeing some of the downsides of the first detector, LLNL and Sandia came up with a second prototype, SONGS2[6].

A third design, SONGS3, does not use a liquid or plastic scintillator. Instead, it uses water mixed with gadolinium and measures Cerenkov light [6]. Cerenkov light, which is mostly ultraviolet but partially blue, is produced when charged particles move faster than the speed of light in water. When the antineutrino collides with a proton, the positron and neutron are created as before. The speeding positron

creates the first flash of light. Again, when the created neutron is captured by the gadolinium nucleus, gamma rays are produced which in turn generate fast Compton scattered electrons and these create a second flash of light.

The SONGS3 detector is a design that has a lot of promise. Because it is made of water, it is much safer than the scintillation liquid. Also, cosmic muons that can mimic an antineutrino signal in scintillator detectors are unable to penetrate the water-based detector. The main drawback of this design is that interactions in water produce less light and it is more difficult for the photomultiplier tubes to detect the fainter signal. Overall, about 100 times fewer Cerenkov photons are created compared with the amount of light found in the liquid and plastic scintillators.

The newest work coming out of the United States is a collaboration between the researchers at LLNL, Sandia and University of Chicago. These researchers are working to develop argon- and germanium-based detectors [6]. These new systems will detect antineutrinos through coherent neutrino-nucleus scattering. The antineutrino collides with the argon or germanium which results in nuclear recoil. When the recoiling nucleus bumps into a neighboring nucleus, a few electrons are freed. The argon-based system then uses a dual-phase detection process where first the electron signal is generated in the liquid argon and then the signal is amplified by an argon gas blanket above the liquid. The amplified signal generates scintillator light which is detected by photomultiplier tubes. The germanium-based detector uses a sensitive transistor to remove and magnify the electrons.

Researchers are very excited by these new proposed designs because coherent scattering has a much higher antineutrino reaction rate per volume compared with inverse beta decay. This would allow for much smaller detectors, possibly

as diminutive as one cubic meter including the shielding. In April 2008, the first germanium-based prototype was installed at SONGS but no results have been released at this time.

2.2 High Temperature Gas-Cooled Reactor

In the 1950s, scientists were experimenting with new ideas for safer and more efficient nuclear powered reactors. They developed the High Temperature Gas-Cooled reactor (HTGR) design. The new design used helium as a coolant instead of water and graphite as a moderator. Using helium allowed the reactors to reach a much higher fuel temperature which made more steam and therefore more energy. Two different types of designs were developed, a prismatic design and a pebble bed. In the US, one reactor of each design was deployed.

2.2.1 *Peach Bottom Reactor*

The Peach Bottom Reactor was located in southwest Pennsylvania and owned by Philadelphia Electric Company. It was the first HTGR prototype in the United States [12]. It ran successfully from June 1967 to October 1974. This pebble bed reactor was helium cooled and graphite moderated but instead of using a prismatic geometry, its fuel consists of small fuel pebbles about the size of a tennis ball. These pebbles each contain about nine grams of uranium. A reactor core contains about 360,000 fuel pebbles with each pebble consisting of 10,000 to 15,000 grains of microsphere coated particles each inside a hard silicon carbide shell. The microspheres are then placed in a graphite matrix. The biggest advantage of this design is that it incorporates online refueling. The new fuel is added while the reactor is still operating and this eliminates the need for the long refueling shutdowns required by other designs (See Figure 5). Each pebble passes through the

reactor an average of six to ten times in a life cycle.

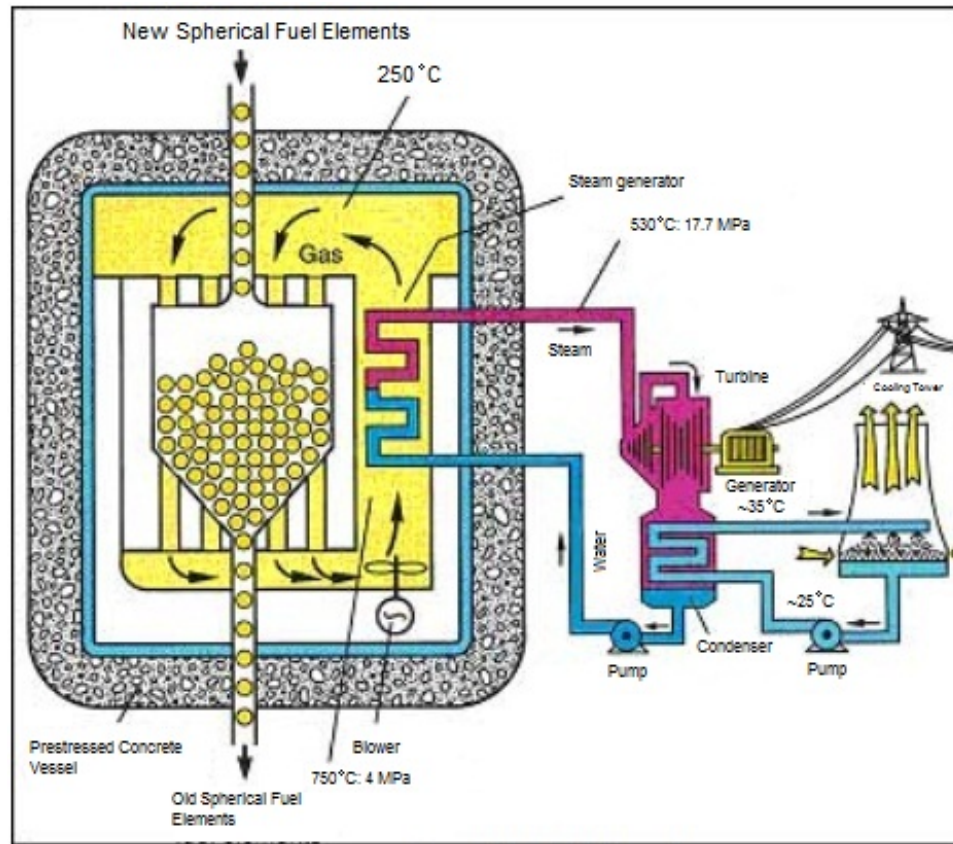


Figure 5: A diagram of a general pebble bed reactor[13].

Peach Bottom was considered a success and was shut down because it had a short-term operating license. Though the reactor worked very well, it was not cost effective to modify it to qualify for a full-term license. By decommissioning it, Peach Bottom also presented a unique opportunity to study the end-of-life conditions in an HTGR. This research was able to help in the validation of HTGR design codes and material behavior.

2.2.2 Fort St. Vrain

The Fort St.Vrain reactor in Colorado reached criticality for the first time on January 31, 1974 [14]. For the entire first year and well into spring of the next year, workers were constantly fixing the control rod drives and cracks in the pelton wheel, which is a type of impulse turbine [15]. There was also a serious problem with moisture ingress into the reactor. The “C” helium circulator also had to be replaced because of an excess of purified helium that had been leaking into the pre-stressed concrete reactor vessel (PCR.V).

On December 11, 1976, Fort St.Vrain produced power for the electricity grid for the first time. For the next eleven months, things ran smoothly until core thermal fluctuations were observed. A small steam generator tube was found to be leaking, and though it was replaced, the fluctuations continued. In October 1979, Lucy Locks, a type of constraint device, were installed to hold the block columns together and stop the fluctuations [16]. This worked, but soon after the “B” helium circulator broke and needed to be replaced. After a few months of normal operations, turbine high vibrations caused a turbine trip, initiating another SCRAM of the reactor. Six months later, the reactor shutdown again for high moisture and during this time two control rods failed to insert and three other rods showed a tendency to stick. The control rod problem was addressed but only three months later, a core support floor tube was found to be leaking. For the next year, the reactor was forced to SCRAM multiple times due to excessive coolant moisture. Once this was finally fixed, the reactor began having multiple problems with the control rod system again. As the control rod system was being repaired, it came to the attention of some of the workers that the helium circulators were beginning to corrode and needed to be repaired or replaced.

In December 1988, the board of directors of Public Service Company, the owners of the reactor, decided to shut down the reactor for good in December of 1990. However, after the announcement, hairline cracks were found in the steel main steam ring header. On August 29, 1989 the reactor was officially shut down and all operations were terminated.

2.2.3 GT-MHR

General Atomics developed the Gas Turbine-Modular Helium Reactor (GT-MHR) to be the safest and most eco-friendly reactor to be designed [17]. The reactor was similar to the Fort St. Vrain design but with a few major modifications. The new design completely eliminated the water-lubricated circulators which were the main difficulty in the previous design. Instead, the GT-MHR uses a highly superior gas-turbine power cycle that fully eliminates the need to create steam.

The design also has much better safety systems in place. The three major nuclear accidents that have occurred have resulted mainly because of a loss of coolant. This new design can withstand a total loss of coolant [18]. Due to the reactor's low power density and geometry, it is physically impossible for the core to meltdown which means that a situation like Three Mile Island or Fukushima would never occur. Knowing this allows the public to feel safer and makes it easier for this design to be approved for building.

2.2.4 VHTR

The Very High Temperature Reactor (VHTR) is the most recent of the gas-cooled reactors. This Generation IV reactor is very similar to its predecessors in many ways including its annular core design (See Figure 6). Its prismatic core is made up of hexagonal moderator and fuel blocks that are arranged in rings [19]. The

inner rings (1-5) form a graphite reflector while the center rings (6-8) contain the active fuel and the outer rings (9-10) form a replaceable graphite reflector. The core is made up of 102, 26-foot tall fuel columns each consisting of ten fuel blocks stacked vertically. In addition to the replaceable reflector, the VHTR also has a permanent side reflector consisting of graphite as well as cooling channels and a core barrel. The primary coolant is helium and it flows into the reactor core and through the coolant channels before it enters the integral coolant channels in the fuel assemblies. This keeps the core even cooler than previous designs.

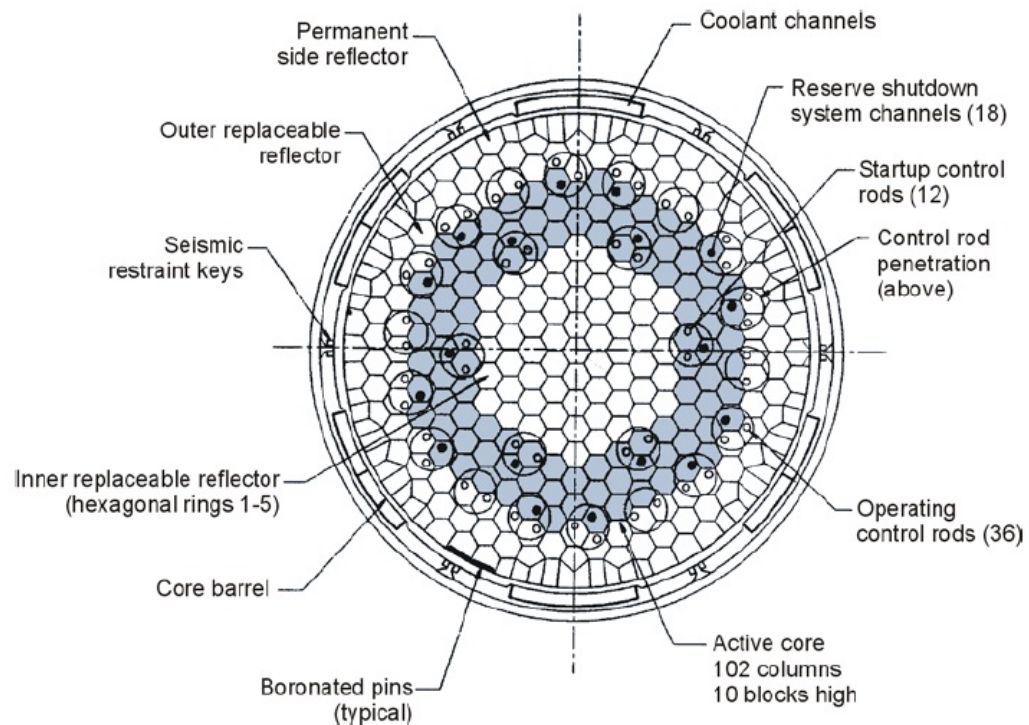


Figure 6: The core of the VHTR still uses the annular design of the GT-MHR [19].

The VHTR uses TRISO fuel particles. This fuel pellet has a UO_2 center with a carbon based outer shell. TRISO fuel has become the fuel of choice for all gas-cooled reactors including both the pebble bed and prismatic designs. More on

TRISO fuel can be found in Section 3.1.

The VHTR uses a closed Brayton cycle to generate electricity through a primary heat transfer loop. Helium flows into the bottom of the core and then up along the inner surface of the core barrel. From there it flows back down the core where it is heated, and then out of the core to the power conversion unit where it is sent through the turbine. A portion of the helium is sent to the Intermediate Heat Exchanger (IHX) to heat the secondary loop and then returns back to the power conversion unit.

As with most of the VHTR, the power conversion unit is very similar to that of the GT-MHR in design. It contains everything necessary for power generation such as the turbine, generator and compressors. These are all installed vertically to make the device smaller and therefore leave a smaller footprint.

Since the primary heat transfer loop is used for electricity generation, the secondary heat transfer loop provides the heat for non-electrical energy products like hydrogen. The secondary loop includes a tertiary heat transfer loop that adds another heat exchanger. This will keep the reactor and hydrogen loops more isolated and avoid contamination. For every reactor, there needs to be a way to remove decay heat. The VHTR design is similar to the GT-MHR in that everything is passive. The reactor cavity cooling system (RCCS) uses cooling panels and an intake/exhaust duct that allow natural-convection air to remove the heat without any human interference.

Because of the major problems at Fort St.Vrain (see Section 2.2.2) with the bearings, the VHTR uses magnetic bearings which prevent the contamination problem. Since the magnetic bearings are not passive, they need electricity to create their electromagnetic field. As a result, catcher bearings are also installed

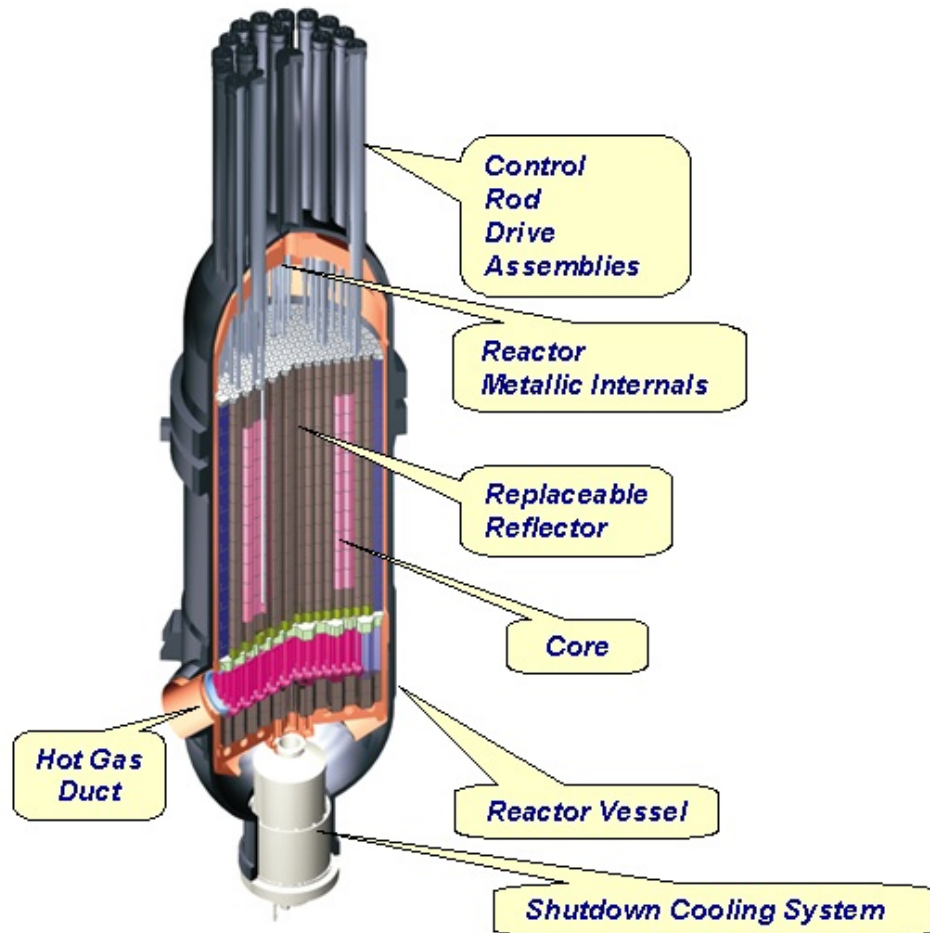


Figure 7: Like the GT-MHR, the VHTR reactor is designed to leave as small of a footprint as possible [19].

for possible drops and coast-downs.

The VHTR is proving to be a good candidate for deployment because of improved safety and reduced cost. However, at this time there are no VHTRs being built for commercial use.

2.3 Research Objectives

Because the spreading of nuclear weaponry is such a large issue in today's world, the Generation IV reactors were designed with nonproliferation goals in mind. Antineutrino detection is another tool to prevent countries from starting or implementing nuclear weapons programs. By simulating the detectors, it is possible to determine the effectiveness of antineutrino detection at this moment in time with HTGRs. This research answers the following questions.

1. Is antineutrino monitoring of a HTGR a valid tool for nonproliferation purposes?
2. What is the impact of additional fertile material in the reactor?
3. Will the change in power distribution cause a detectable antineutrino signature?

3 Materials and Methods

3.1 TRISO Fuel

Pebble Bed reactors and prismatic reactors both use the same kind of fuel. Tri-Structural-Isotropic (TRISO) fuel [20] is made up of ceramic coated fuel particles and has proven to be safer with higher temperatures (See Figure 8). The fuel particle is made up of five layers. The center is the fuel kernel, normally UO_2 or UCO. Surrounding the kernel is a pyrolytic carbon buffer layer. This buffer layer is porous and therefore able to allow fission products to pass through. Outside of these layers are the three structural layers from which the fuel gets its name. The innermost layer of the three is made up of IPyC and the outermost layer is constructed of OPyC. These are both a high density pyrolytic carbon and protect the inner layer from corrosive gases often used in the layer between the two. Between the two layers resides a layer of silicon carbide (SiC). The SiC acts as both a pressure vessel for the particle by withstanding the internal gas pressure buildup and also as a diffusion barrier to gaseous and metal fission products.

The fuel particles are tiny. Each fuel particle is $530 \mu\text{m}$ in diameter, on average [21]. These fuel particles are compressed together into a compact that is about 1.245 cm in diameter. These compacts are then placed in a graphite matrix to make up a hexagonal fuel assembly that is inserted into the core of the reactor. See Figure 9 to get an idea of size comparisons.

TRISO fuel is known for being much safer than traditional reactor fuels. Because of its unique design, a HTGR can run at a much lower power density than typical light water reactors, usually anywhere from 3-4 MW/m^3 [21]. The lowest power density is found in the buffer layer because it has the smallest density.

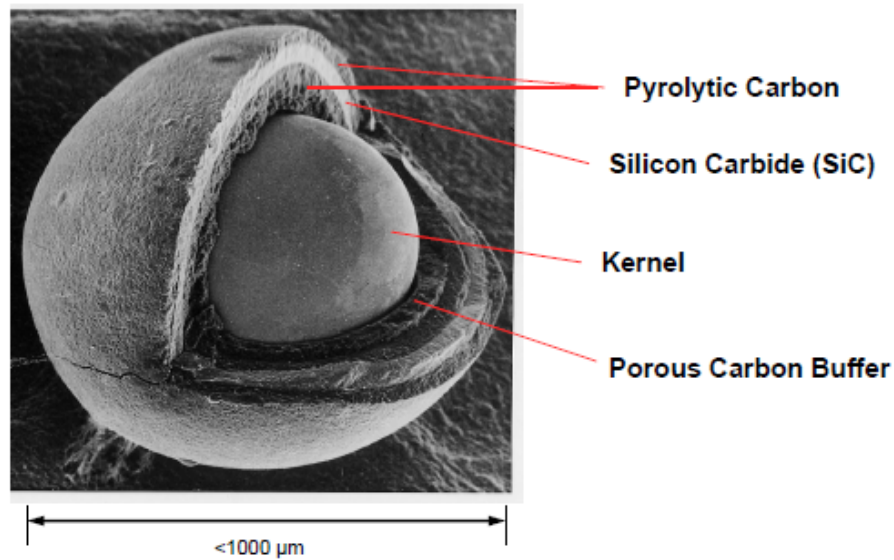


Figure 8: A TRISO kernel is made up of different layers which work together to combat the extreme temperatures[22].

As with every technology, TRISO fuel does have its shortcomings. It is possible for the fuel particles to fail. Manufacturing defects and imprecision are always going to be a factor in technology. However, TRISO fuel has been known to have other maladies. These failures fall into two categories [22], mechanical and chemical. Mechanical failures include those where a structural layer fails as a result of stress. There are two different causes to stress fractures in the fuel. Over pressure failures occur when fission products build up inside the kernel. Some of the fission products, mainly Xe and Kr, are gaseous and travel out of the kernel into the outer layers. These gases build up pressure and can exceed the strength of one of the layers. When one layer fails, the fuel particle is useless. A second mechanical failure is called Cracking Induced Failure [20]. This occurs when the pyrocarbon shrinks both radially and tangentially during irradiation. During prolonged exposure to radiation, the pyrocarbon begins to reorient and swell radially while still shrinking

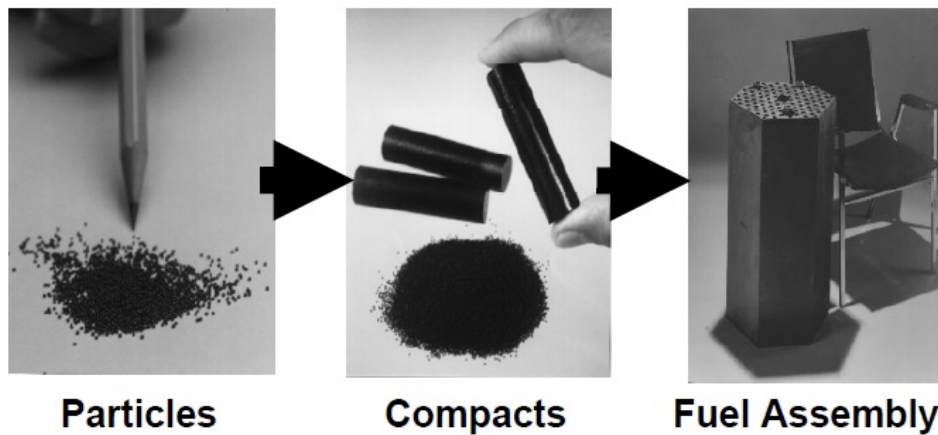


Figure 9: TRISO fuel particles are tiny. They are first compressed together to form a compact and then the compacts are arranged to create a fuel assembly[23].

tangentially. This causes the pyrocarbon layers to crack which in turn causes the SiC layer to crack and compromises the fuel particle.

Chemical failures can also be categorized into two different types [22]. Fission Product Attacks are caused when fission products are built up and then released from the kernel. These products create a certain amount of corroding in the structural layers depending on the amount of free oxygen and the temperature of the fuel. The higher the temperature the more corrosion occurs. Obviously, this corrosion compromises the strength of the structural layers and they fail. The second chemical failure type is called the Amoeba Effect. For an example, see Figure 10. This occurs when the fuel kernel is thermally driven toward the hot side of the microsphere. This is a slow process that occurs at higher temperatures. When using an oxide fuel, the oxygen reacts with PyC to form carbon monoxide (CO). The CO moves to the cold side of the microsphere which pushes the kernel to the hot side. In severe cases, the kernel can actually collide with or break through the structural layers.

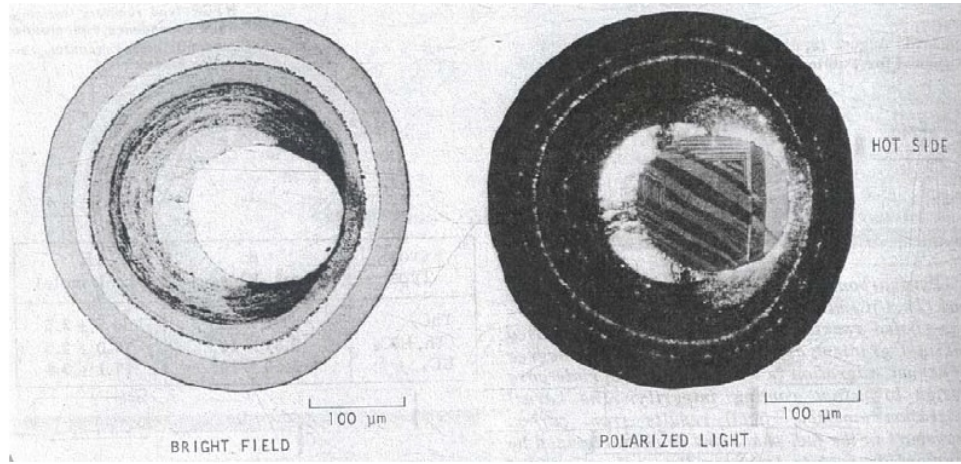


Figure 10: The Amoeba Effect occurs when the fuel kernel is thermally driven toward the hot side of the microsphere[20].

3.2 NEWT

To determine the usefulness of antineutrino detectors with an HTGR, the first step is to simulate a depleted assembly. SCALE 6.1 was chosen for this task because of its simplicity in use as well as its consistency with other more well known methods such as Serpent and Monte Carlo N-Particle Transport Code (MCNP) (see Figure 11). It was also used because of its ability to work with double heterogenous fuel such as TRISO.

SCALE 6.1 is a package of codes used to simulate nuclear reactors. NEWT is the code used for transport calculations[24]. It begins with the time-independent form of the linear transport equation

$$\hat{\Omega} \cdot \vec{\nabla} \Psi(\vec{r}, \hat{\Omega}, E) + \Sigma_t(\vec{r}, E) \Psi(\vec{r}, \hat{\Omega}, E) = Q(\vec{r}, \hat{\Omega}, E) \quad (2)$$

where

$\Psi(\vec{r}, \hat{\Omega}, E) \equiv$ angular flux at position \vec{r} in direction $\hat{\Omega}$ at energy E

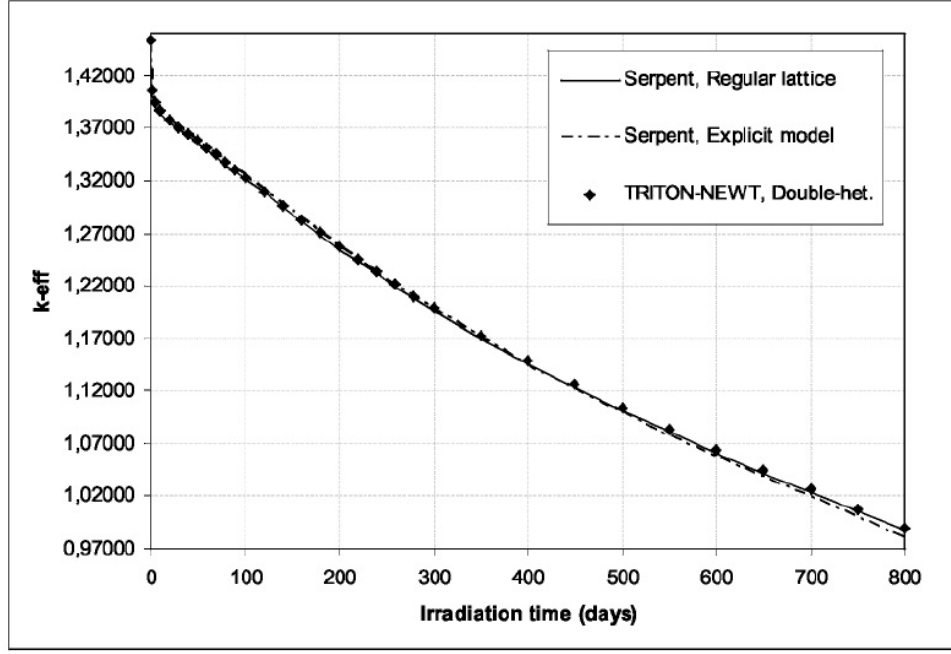


Figure 11: Comparison of burnup calculations found by use of Serpent and TRITON-NEWT for a prismatic block without burnable poison.[25].

$\Sigma_t(\vec{r}, E) \equiv$ total macroscopic cross section at position \vec{r} and energy E

$Q(\vec{r}, \hat{\Omega}, E) \equiv$ source at position \vec{r} , in direction $\hat{\Omega}$ at energy E.

The source, Q, is made up of three terms including the scattering term

$$S(\vec{r}, \hat{\Omega}, E) = \int_{4\pi} d\hat{\Omega}' \int_0^\infty dE' \Sigma_s(\vec{r}, \hat{\Omega}' \rightarrow \hat{\Omega}, E' \rightarrow E) \Psi(\vec{r}, \hat{\Omega}', E') \quad (3)$$

where

$\Sigma_s(\vec{r}, \hat{\Omega}' \rightarrow \hat{\Omega}, E' \rightarrow E) \equiv$ macroscopic scattering cross sections at \vec{r}

from beginning E' and $\hat{\Omega}'$ to final E and $\hat{\Omega}$,

a fission source

$$F(\vec{r}, \hat{\Omega}, E) = \frac{1}{4\pi} \chi(\vec{r}, E) \int_0^\infty dE' \nu(\vec{r}, E') \Sigma_f(\vec{r}, E') \Psi(\vec{r}, \hat{\Omega}, E') \quad (4)$$

where

$$\Sigma_f(\vec{r}, E') \equiv \text{macroscopic fission cross section at } \vec{r} \text{ and } E',$$

$\nu(\vec{r}, E') \equiv$ number of neutrons released per fission caused by a neutron at \vec{r} and energy E' ,

$$\chi(\vec{r}, E) \equiv \text{fraction of fission neutrons that are born at } \vec{r} \text{ and } E$$

as well as an outside or fixed source, $W(\vec{r}, E)$.

Typically, the transport equation is very difficult to solve analytically for anything other than a highly idealized case. Because of this, NEWT simplifies and approximates using the Extended Step Characteristic (ESC) discretization method [26]. For example, it is impossible to exactly represent a cylinder in a 2-D Cartesian coordinate system; so instead, NEWT will approximately decompose the cylinder into a number of rectangular cells.

NEWT starts the process by solving the transport equation analytically along characteristic directions within one of the computational cells. The angular flux Ψ is solved along a coordinate in direction $\hat{\Omega}$ and simplifies the streaming term to

$$\hat{\Omega} \cdot \vec{\nabla} \Psi(\vec{r}, \hat{\Omega}, E) = \frac{d\Psi(s, E)}{ds} \quad (5)$$

Now the transport equation can be simplified to

$$\frac{d\Psi(s)}{ds} + \Sigma_t(s)\Psi(s) = Q(s) \quad (6)$$

which, with the assumption that Q and Σ_t are spatially constant, has a solution

$$\Psi(s) = \Psi_0 e^{-\Sigma_t s} + e^{-\Sigma_t s} \int_0^s Q e^{\Sigma_t s'} ds' \quad (7)$$

where s is the distance in direction $\hat{\Omega}$ and Ψ_0 is the known angular flux at $s=0$. From boundary conditions for known cells, Ψ_0 is a known entity and other angular fluxes can be found from Eqn 7.

NEWT uses the Step Characteristic method to find the appropriate value for Ψ_0 . Using this technique, the source, Q , and the macroscopic total cross section, Σ_t , are assumed to be constant within the computational cell, and the angular flux is assumed to be constant at the cell boundaries. By integrating Eqn 7, it is found that

$$\Psi(s) = \Psi_0 e^{-\Sigma_t s} + \frac{Q}{\Sigma_t} (1 - e^{-\Sigma_t s}). \quad (8)$$

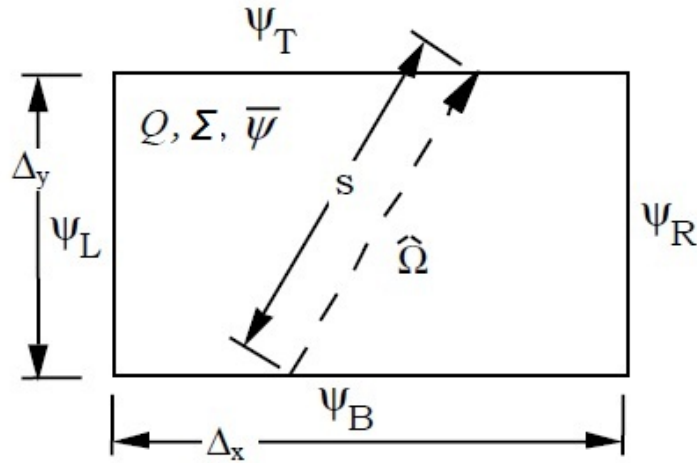


Figure 12: A representative computational cell to use as a visual when deducing how NEWT solves the transport equation[24].

Figure 12 shows an example of a hypothetical computational cell. For a given direction, $\hat{\Omega}$, the angular flux on any unknown side can be determined by taking an average of the fluxes from the known sides. For example, the unknown flux, Ψ_T , can be found by taking the linear weighted average from known sides Ψ_L and

Ψ_B . Because these fluxes are assumed to be constant along the side, they can be used to find the missing side which is assumed to be the average in the direction $\hat{\Omega}$.

Because the characteristic directions are chosen from a quadrature set, the resulting angular fluxes can be integrated over angle to find scalar fluxes. By knowing the lengths of the sides of a computational rectangular cell (Δx and Δy) and the directions cosines of $\hat{\Omega}$, the length, s , can be determined. The solution to Eqn 8 can then be integrated along the length of each unknown side to determine the unknown sides average angular flux. Once all the sides are known, the average angular flux for the entire cell can be found.

NEWT also employs a coarse-mesh finite-difference acceleration (CMFD) approach [27]. This process homogenizes selected rectangular regions and then uses coupling correction factors for each of the rectangular cells to estimate the transport solution for the polygonal cells. It also takes multiple groups and collapses them so that two-group calculations can be performed. The simplified formulation leads to faster convergence and less time taken for the problem to finish.

This is just a very basic description of what NEWT does. This method assumes the computational cells are rectangular but this is not a necessity. For other geometries to be used, it simply needs to know the relationship between cell edges in the direction of the characteristic. For an illustration of how NEWT works, see Appendix C.

3.3 Core Simulations

The first step for modeling the core of the reactor was to deplete a single assembly. Once it was apparent that the assembly was depleting correctly, it became possible

to deplete multiple assemblies at different power densities so that the data for a core depletion could be determined. These power densities were calculated by using assembly pin peaking factors for each ring that had been found previously by researchers at Idaho National Laboratory who were attempting to answer questions that had risen from the use of TRISO fuel. These pin peaking factors can be seen in Appendix B. From that initial data, averaging the pin peaking factor across the assembly led to the power level relative to the norm for each ring of assemblies in the core. This relative power level was then multiplied by the normal power density to find the power density of each assembly. Overall, the power distribution was fairly flat, which makes sense since the fuel region has a reflector on both the inner and outer edges.

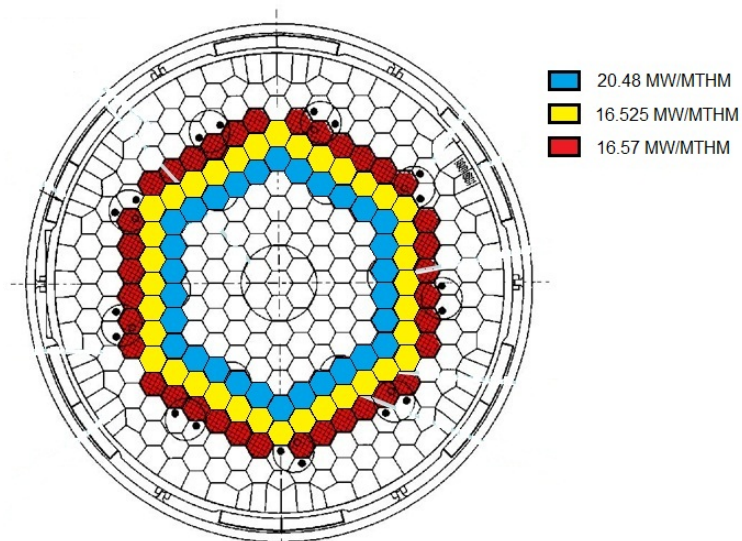


Figure 13: The power distribution by ring in the core[28].

Most nuclear reactors have an enrichment distribution across the core to even out the power. However, simulations thus far on the NGNP have kept a uniform enrichment to simplify particle fabrication and testing requirements to license the

fuel [29]. Because of this, these simulations were also run with a uniform enrichment over one fuel cycle. The original enrichment for the reactor is 11.7%. The reactor has a fuel temperature of 950° C. Each fuel block is prismatic in design with a diameter of 0.36m, a height of 0.8m and made up of 2862 fuel compacts (see Figure 14). Each fuel compact is 0.9398cm in diameter and 4.93cm tall. The entire core is made up of 1020 fuel blocks and has a total height of eight meters.

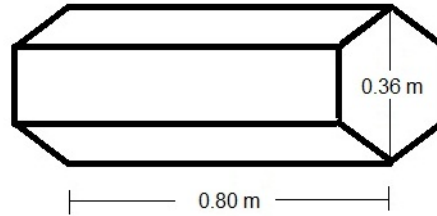


Figure 14: A single fuel compact.

Each simulation was performed using a 44 group solution and ten depletion steps with a spatial mesh of 31x18 over 547 days (one fuel cycle). This was done for varying enrichments and power levels.

3.4 Antineutrino Detector

While the primary goal of this thesis is to determine antineutrino source terms for a HTGR, a secondary purpose is to examine how an antineutrino detector will respond when placed nearby. Using the information from the SONGS1 detector, it is assumed that the detector is located 25 meters away from and ten meters below the reactor. From this data, the antineutrino source term was geometrically attenuated to determine the source term at the reactor. By factoring in the average interaction rate of one interaction for every 2.5×10^{13} antineutrinos, the number of antineutrino interactions per second in the detector was calculated. Because this

number was less than one interaction per second, the rate was changed to interactions per day. While SONGS1 has an efficiency ($\epsilon = \frac{\text{counts detected}}{\text{interactions}}$) of 10%, other detectors have much higher efficiencies, some as high as 50%. The calculated interactions/day was multiplied by these various efficiencies to best determine number of counts the detectors would collect. This is demonstrated in Eqn 9.

$$\frac{\bar{\nu}}{s} \times \frac{1}{4\pi r^2} \times \frac{1 \text{ interaction}}{2.5 \times 10^{13} \bar{\nu}} \times \frac{60s}{1 \text{ min}} \times \frac{60 \text{ min}}{1 \text{ hr}} \times \frac{24 \text{ hr}}{1 \text{ day}} \times \epsilon = \frac{\text{counts}}{\text{day}} \quad (9)$$

3.5 Verification of Results

To verify that the data was accurate, test simulations were performed to make sure the results converged. To do this, several more trials were carried out for a single assembly but using different parameters. These new trials included changing the number of energy groups from 44 to 238, changing the number of depletion steps from ten to four, changing the quadrature order from the original number, six, three different times ($S_N=4,8,10$) and finally changing to a larger mesh size. From the new trial data, the antineutrino source term was calculated and then compared to the original simulation and the percent difference was found between the two resulting outputs at each time step. From these percentages, a mean and a median percent difference was calculated.

As can be seen in Table 1, the different simulations all gave very similar output data. To see the difference in the spatial mesh grid, see Figure 15. The largest difference occurred when changing the group set used from 44 to 238. This led to a six percent decrease in the antineutrino source term for the single assembly. However, since this decrease is universal, it does not affect the conclusion reached from the results.

Table 1: Checking convergence of different simulations by changing different parameters.

		Depletion Steps	Mesh	S_4	S_8	S_{10}	Energy Groups
U-235	Mean	1.06%	0.01%	0.49%	0.46%	0.45%	6.38%
	Median	1.10%	0.01%	0.50%	0.46%	0.46%	6.41%
U-238	Mean	1.06%	0.01%	0.49%	0.46%	0.45%	6.39%
	Median	1.07%	0.01%	0.50%	0.46%	0.46%	6.41%
Pu-239	Mean	1.20%	0.03%	0.55%	0.50%	0.52%	6.54%
	Median	1.22%	0.01%	0.58%	0.50%	0.54%	6.56%

4 Results

Once the simulations were completed and the data analyzed, antineutrino counts were estimated based on the flux and the atomic densities of the different isotopes. The original simulation, using known operating parameters for a HTGR, attested to the fact that the simulation was performing in a way that made sense logically. (See Figure 16.) The amount of ^{235}U decreased while the ^{238}U held steady. Also, ^{239}Pu is produced as a result of neutron capture reactions with ^{238}U . This all was expected and demonstrated that the simulation tool was working correctly and would be able to estimate the antineutrino source term for different scenarios.

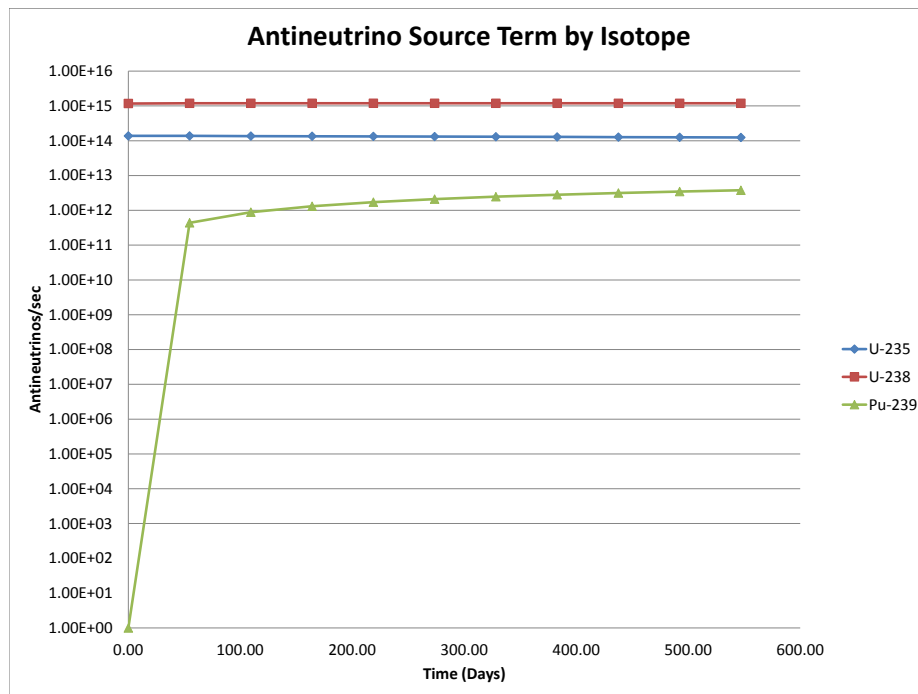


Figure 16: Antineutrino source term by isotope for normal reactor operating parameters.

4.1 Changing Enrichment

To produce a higher antineutrino rate, simulations were run with lower fuel enrichments. (See Figure 18 and 19.) The original simulation was run with a uniform BOC enrichment of 11.7% for one fuel cycle. This was repeated in the second simulation but with an enrichment of 9.5%. A third simulation was run with an enrichment of 8%. The results of the simulations were then broken down by antineutrino source term by isotope per assembly. From knowing the antineutrino source term of an assembly in each fuel ring, the antineutrino source term for the entire core was calculated. Since a lower enrichment should lead to a higher number of plutonium antineutrinos, this was a way to make sure the simulations were running correctly. By looking at the graphs, it is obvious that a lower enrichment does lead to a larger total number of antineutrinos as well as a larger number of antineutrinos from plutonium.

Table 2: Percent difference in antineutrino source term with changes in enrichments.

Time (day)	ν/s at 11.7% Enrichment	ν/s at 9.5% Enrichment	Difference	ν/s at 8.0% Enrichment	Difference
0.0	1.43E10	1.58E10	10.12%	1.72E10	20.37%
54.7	1.45E10	1.59E10	10.08%	1.74E10	20.07%
109.4	1.45E10	1.59E10	9.95%	1.73E10	19.77%
164.1	1.45E10	1.59E10	9.80%	1.73E10	19.47%
218.8	1.45E10	1.59E10	9.71%	1.73E10	19.26%
273.5	1.45E10	1.58E10	9.54%	1.72E10	18.94%
328.2	1.45E10	1.58E10	9.38%	1.71E10	18.63%
382.9	1.44E10	1.58E10	9.30%	1.71E10	18.37%
437.6	1.44E10	1.57E10	9.19%	1.70E10	18.15%
492.3	1.44E10	1.57E10	9.15%	1.70E10	17.99%
547.0	1.44E10	1.57E10	9.06%	1.69E10	17.87%
		Average	9.57%		18.99%
		Median	9.54%		18.94%

After adjusting for geometric attenuation as well as the efficiency of the SONGS1

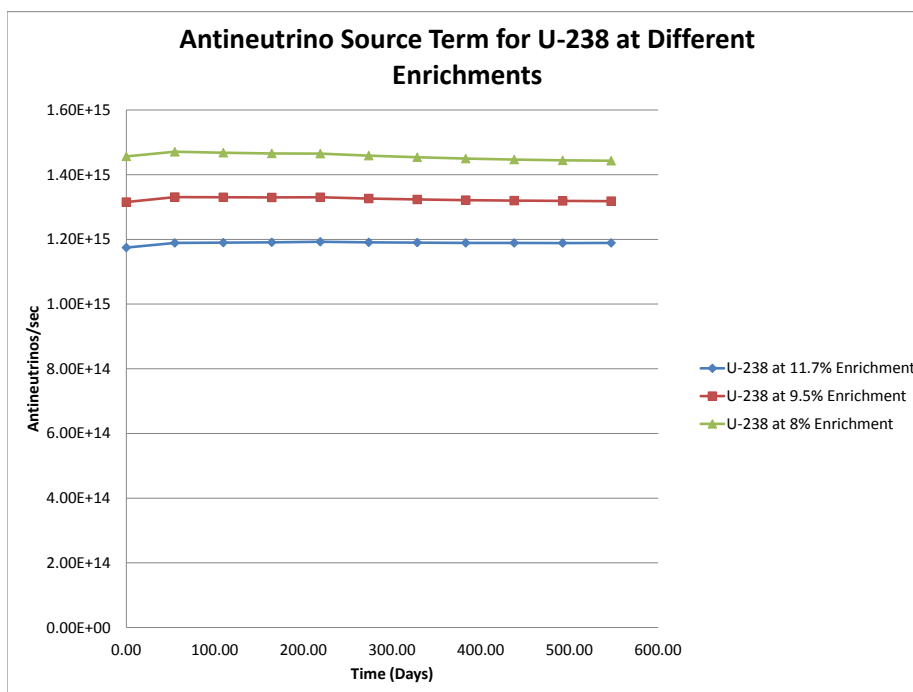


Figure 17: Antineutrino rate of U-238 when changing the enrichment of the fuel.

detector, an average difference of 9.54% was found when the core was made up of 9.5% enriched fuel. When the enrichment dropped even further to 8.0%, the average difference shot up to 18.99%. Because anything less than a 5% change can be attributed to natural fluctuations of the reactor, it is significant that the difference is large enough to distinguish between normal and unusual operating parameters. At almost 10% and 20%, it would be easy for anyone monitoring this reactor to be able to tell if the reactor is being run with a much lower enrichment.

In addition to this, changing the enrichment leads to a difference in shape of the antineutrino source term. The lower enrichments have a steeper declining slope. This can be seen later in Figure 23. The number of antineutrinos being produced decreases at a faster rate than the higher enrichments. This would be another way

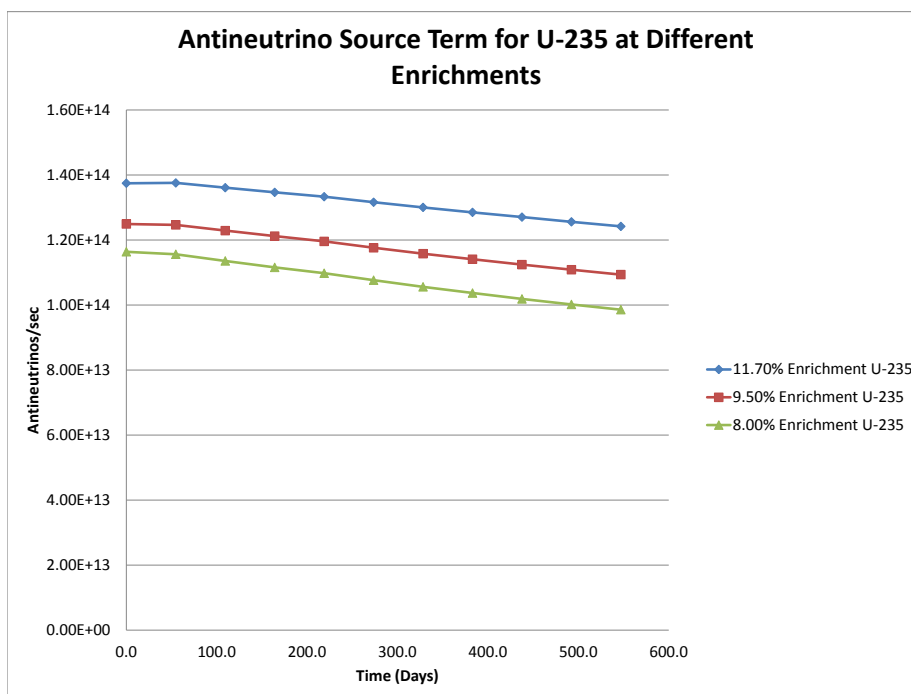


Figure 18: Antineutrino rate of U-235 when changing the enrichment of the fuel.

to determine if the reactor is being operated using unusual parameters.

4.2 Changing Power Levels

In another attempt to see if the SONGS detector would be effective at determining whether or not a reactor was being used to produce extra plutonium, the simulations were performed again but at a higher power level. (See Figures 21 and 22.) Increasing the power level will increase the plutonium production and therefore will increase the number of antineutrinos. Two extra simulations were run, one at five percent power increase and the other at ten percent power increase. Both simulations were run with original BOC parameters, including a universal enrichment of 11.7%.

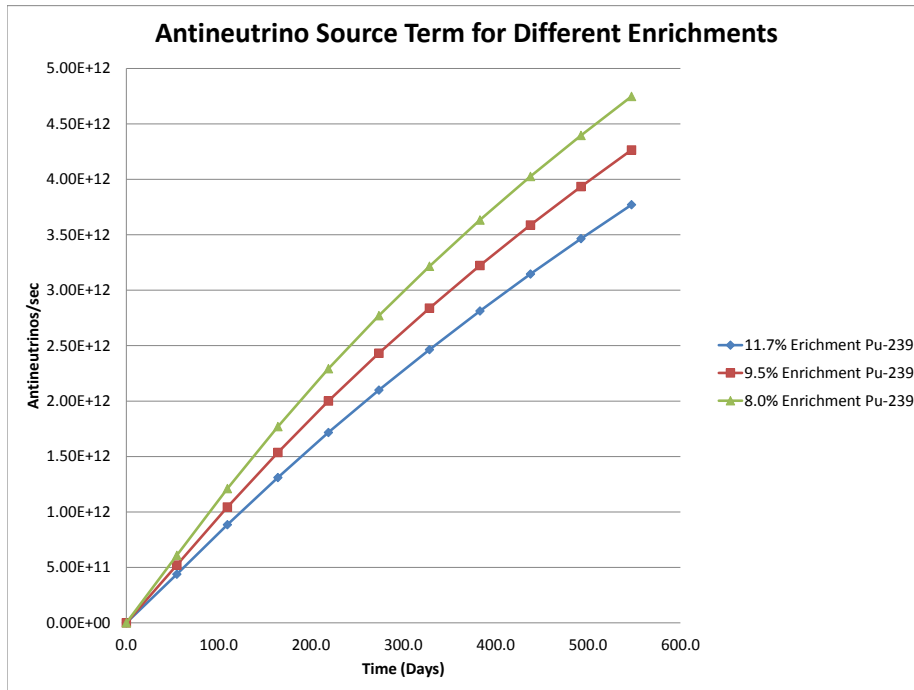


Figure 19: Antineutrino rate of Pu when changing the enrichment of the fuel.

Once geometric attenuation and detector efficiency were factored in, a pattern became apparent. Whatever percentage the power was increased, the antineutrino source term seemed to increase by the same percentage. This meant that for a 5% increase in power, the antineutrino rate increased by 5%. The same thing happened with a 10% increase in power. This pattern implies that if the reactor is running at a power level greater than 5% above normal, SONGS1 would be able to detect the irregularity.

4.3 Antineutrino Detector

By determining geometric attenuation as well as using the average antineutrino interaction rate, it was possible to determine the number of counts a detector would record per day over the fuel cycle. This was varied to account for different

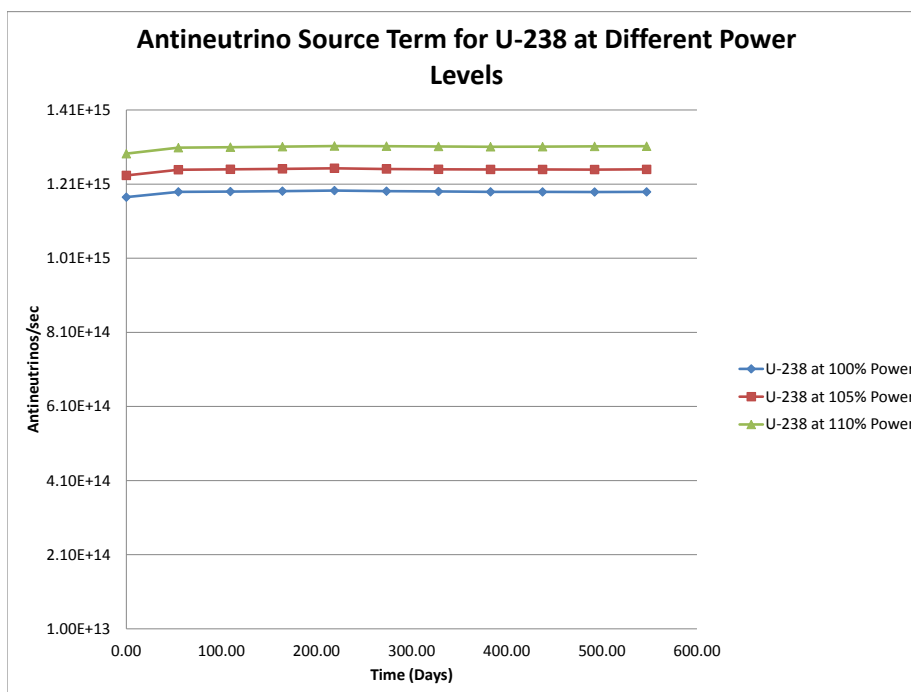


Figure 20: Antineutrino rate of U-238 when changing the power density of the reactor.

detector efficiencies. Three different sets of calculations were made: the original operating parameters, a decrease to eight percent enrichment, and an increase to 110% power. The results can be seen in Table 4.

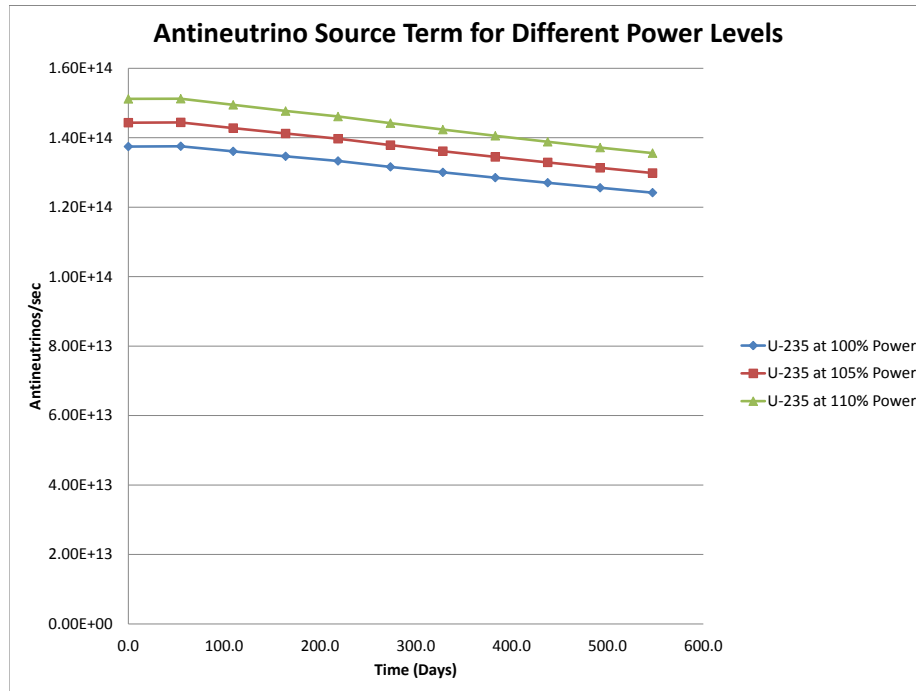


Figure 21: Antineutrino rate of U-238 when changing the power density of the reactor.

Table 3: Percent difference in antineutrino source term with changes in power levels.

Time (day)	ν/s at 100% Power	ν/s at 105% Power	Difference	ν/s at 110% Power	Difference
0.0	1.43E10	1.5040E10	5.00%	1.58E10	10.00%
54.7	1.45E10	1.52E10	5.03%	1.59E10	10.04%
109.4	1.45E10	1.52E10	5.04%	1.59E10	10.06%
164.1	1.45E10	1.52E10	5.04%	1.59E10	10.07%
218.8	1.45E10	1.52E10	5.03%	1.60E10	10.07%
273.5	1.45E10	1.52E10	5.02%	1.59E10	10.17%
328.2	1.44E10	1.52E10	5.01%	1.59E10	10.17%
382.9	1.44E10	1.51E10	5.05%	1.59E10	10.19%
437.6	1.44E10	1.51E10	5.06%	1.59E10	10.21%
492.3	1.44E10	1.51E10	5.06%	1.59E10	10.28%
547.0	1.44E10	1.51E10	5.06%	1.59E10	10.28%
		Average	5.04%		10.14%
		Median	5.04%		10.17%

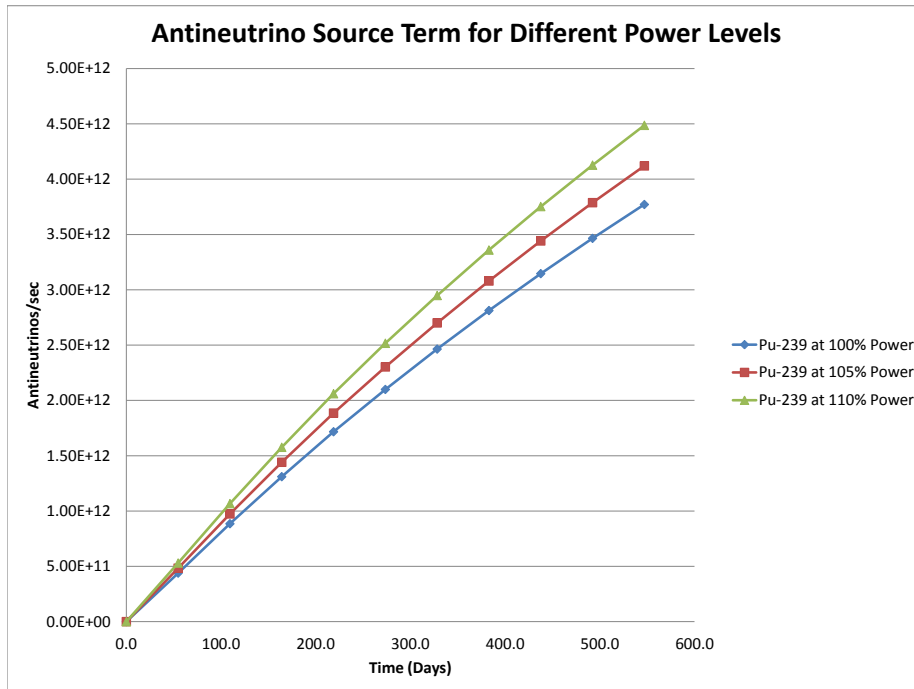


Figure 22: Antineutrino rate of Pu when changing the power density of the reactor.

Table 4: Detector Antineutrino Counts Per Day

Time (days)	Original Parameters			8% Enrichment			110% Power		
	10% ϵ	20% ϵ	50% ϵ	10% ϵ	20% ϵ	50% ϵ	10% ϵ	20% ϵ	50% ϵ
0.0	498	996	2489	597	1193	2983	548	1095	2738
54.7	503	1007	2517	602	1204	3010	554	1108	2770
109.4	503	1007	2517	600	1201	3002	554	1108	2770
164.1	503	1007	2517	599	1198	2995	554	1108	2770
218.8	504	1007	2518	598	1197	2991	554	1108	2771
273.5	502	1005	2512	595	1191	2977	554	1107	2768
328.2	502	1003	2509	593	1186	2964	553	1105	2763
382.9	501	1002	2504	591	1181	2953	552	1104	2759
437.6	500	1001	2502	589	1178	2945	551	1103	2757
492.3	500	1000	2499	588	1175	2938	551	1102	2756
547.0	500	999	2498	587	1173	2933	551	1102	2754

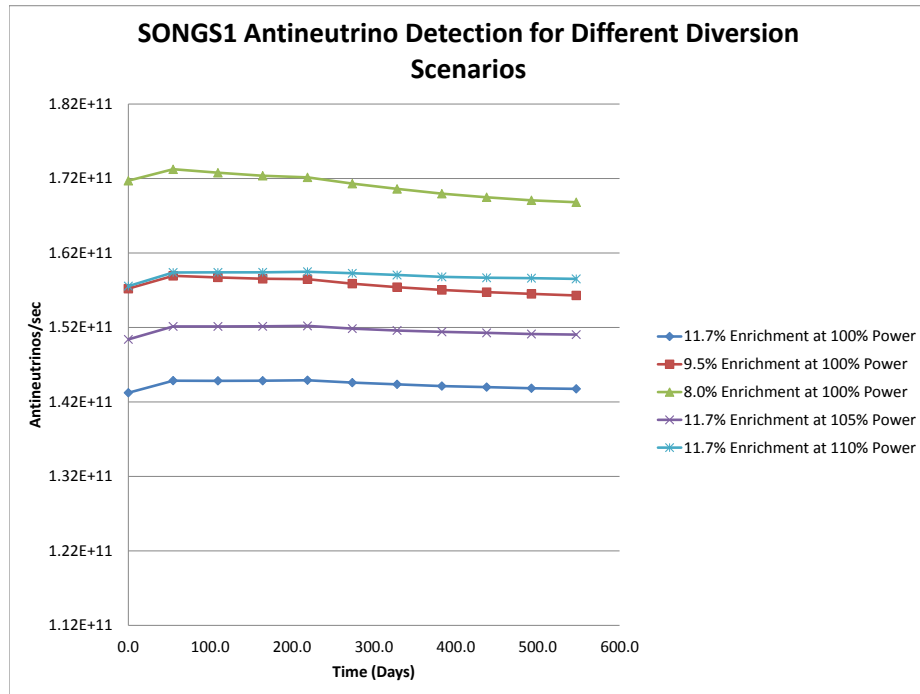


Figure 23: Total number of antineutrinos for each simulation.

5 Conclusions

5.1 Discussion of Results

To determine the effectiveness of an antineutrino detector for nonproliferation purposes, multiple diversion scenarios were simulated and the data from these simulations analyzed. By introducing a lower enriched fuel into the BOC, a higher antineutrino source term is found. The difference in antineutrino output for a 2.2% lower enrichment is well above the 5% needed to clearly identify a change in antineutrino output. A detector would be able to determine the irregular use of the reactor with plenty of time for inspectors to come in and stop any plutonium stockpiling. An enrichment closer to the 11.7% used in normal operations will have a smaller percent change and could be more difficult to detect. However, that smaller change in enrichment would also produce less plutonium, therefore reducing the proliferation risk of this scenario, if the reactor is operated at the same power level.

Higher power densities also are shown to be a good indicator of plutonium production. The percentage of antineutrinos detected increases linearly with the percentage increase in power level. If the reactor is being operated at a 5% power increase, the antineutrino detector would be able to identify this difference quickly and inspectors can be sent in. However, anything less than a 5% increase in the power level will not be detectable.

While the primary focus of this thesis is establishing an antineutrino source term for a HTGR, a secondary aspect is determining the effectiveness of an antineutrino detector placed near the reactor. As seen in the calculated data, a SONGS1 detector is able to record enough counts to distinguish between different

diversion scenarios. To detectors with higher efficiencies, it would be even more apparent when a reactor is being operated with unusual parameters.

5.2 Future Work

The largest problem with this research is that there is no working reactor with which to compare results. Because of this, it is difficult to determine how accurate the results are. Because of this, it was necessary to determine at every step that the results still made logical sense. Future work would necessitate better comparisons with data from an actual reactor once one has been operated. It would even be better if there was more HTGR data available for comparison however a lot of that data is not being shared yet.

Another improvement would be better enrichment data. All simulations were performed with uniform enrichments because the distribution of the assemblies by enrichment was not available at this time. When more is known about the new reactor, it would be advisable to complete the simulations with the new enrichment spectrum.

Bibliography

- [1] International Atomic Energy Agency, “About Us”, *www.iaea.com*, 2011.
- [2] N.S. Bowden, “Reactor Monitoring and Safeguards Using Antineutrino Detectors”, *Journal of Physics*, Conference Series 136, 2008.
- [3] G. Mention, “Double Chooz Near Detector”, Conference Presentation, *Workshop AAP*, CEA Saclay, France, December 14, 2007.
- [4] J.C. Anjos, A.F. Barbosa, T.J.C. Bezerra, P. Chimenti, L.F.G. Gonzalez, E. Kemp, M.A. Leigui de Oliveira, H.P. Lima Jr., R.M. Lima & H. Nunokawa, “The Angra Project: Monitoring Nuclear Reactors with Antineutrino Detectors”, IAEA-CN-184/7, American Institute of Physics, 2010.
- [5] F. Suekane, “KASKA and Its Prototype”, Conference Presentation, *Applied Antineutrino Physics Workshop*, December 13-14, 2007, APC Paris, France, 2007.
- [6] C. Meissner, “Antineutrino Detectors Improve Reactor Safeguards”, *Science and Technology Review*, July/August 2008, Lawrence Livermore National Lab, 2008.
- [7] M. Neito, A. Hayes & W. Wilson, “Detection of Antineutrinos for Non-proliferation”, *Nuclear Science and Engineering*, **149**, pp 270-276, 2005.
- [8] N.S Bowden, A. Bernstein, S. Dazeley, R. Svoboda, A. Meissner & T. Palmer, “Observation of the isotopic evolution of pressurized water reactor fuel using an antineutrino detector”, *Journal of Applied Physics*, **105**, 064902, 2009.
- [9] N.S Bowden, A. Bernstein, A. Meissner & T. Palmer, “Monitoring the Thermal Power of Nuclear Reactors with a Prototype Cubic Meter Antineutrino Detector”, *Journal of Applied Physics*, **103**, 074905, 2008.
- [10] V. Bulaevskaya & A. Bernstein, “Detection of Anomalous Reactor Activity Using Antineutrino Count Evolution Over the Course of a Reactor Cycle”, *Journal of Applied Physics*, **109**, 114909, 2011.
- [11] A. Bernstein, G. Baldwin, B. Boyer, M. Goodman, J. Leanred. D. Reyna & R. Svoboda, “Nuclear Security Applications of Antineutrino Detectors: Current Capabilities and Future Prospects”, *Science and Global Security*, **18**, pp 127-192, 2010.

- [12] J.L. Everett & E.J. Kohler, “Peach Bottom Unit No. 1: A High Performance Helium Cooled Nuclear Power Plant”, *Annals of Nuclear Energy*, **5**, Issues 8-10, pp 321-335, 1978.
- [13] KernEnergie, “Pebble Bed Reactor”, Informationskreis KernEnergie, Berlin, www.kernenergie.de, 2011.
- [14] Fort St. Vrain Folks, “Fort St. Vrain Power Plant History”, <http://www.fsvfolks.org/>, 2011.
- [15] J.B. Calvert, “Turbines”, University of Denver, July 23, 2003, <http://mysite.du.edu/jcalvert/>, 2012.
- [16] S. Perle, “Fort St. Vrain”, *Rad Safe Query*, Global Dosimetry Solutions, December 17, 2007.
- [17] A. Kiryushin & N. Kodochigov, “GT-MHR Project”, HTR-2002-105, OKB Mechanical Engineering, 2008.
- [18] General Atomics, “GT-MHR: Inherently Safe Nuclear Power For the 21st Century”, Energy Home, <http://gt-mhr.ga.com/>, 2011.
- [19] D. Chapin, S. Kiffer and J. Nestell, “The Very High Temperature Reactor: A Technical Summary”, Revision 0, June 2004, MPR Associates Inc., 2004.
- [20] J. Powers, “An Introduction to Current Reactor Design Trends”, Masters Thesis for University of California, Berkeley, 2009.
- [21] J. Hu, R. Uddin, “3D Thermal Modeling of TRISO Fuel Coupled with Neutronic Simulation”, LA-UR-10-00442, Los Alamos National Laboratory, New Mexico, 2003.
- [22] M.A. Stawicki, “Benchmarking of the MIT High Temperature Gas-Cooled Reactor TRISO-Coated Particle Fuel Performance Model”, Masters Thesis for Massachusetts Institute of Technology, 2006.
- [23] D. Petti, “Module 7a: TRISO Fuel Design, Properties, and Requirements”, Conference Presentation, *HTGR Technology Course for the Nuclear Regulatory Commission*, May 24-27, 2010, Idaho National Laboratory & US National Regulatory Commission, 2010.
- [24] M.D. DeHart, “NEWT: A New Transport Algorithm for Two-Dimensional Discrete Ordinates Analysis in Non-Orthogonal Geometries”, *SCALE 6.1 Manual*, Oak Ridge National Laboratory, Tennessee, 2009.

- [25] J. Lappanen & M.D. DeHart, “HTGR Reactor Physics and Burnup Calculations Using the Serpent Monte Carlo Code”, *Trans. Am. Nucl. Soc.*, **101**, 2009.
- [26] M.D. DeHart, “Advancements in Generalized-Geometry Discrete Ordinates Transport for Lattice Physics Calculations”, Conference Presentation, *Proc. of PHYSOR2006, American Nuclear Society Topical Meeting on Reactor Physics: Advances in Nuclear Analysis and Simulation*, September 10-14, 2006, Vancouver, BC, Canada, 2006.
- [27] Z. Zhong & M.D. DeHart “Coarse-Mesh Finite-Difference Acceleration in the NEWT Generalized-Geometry Lattice Physics Package”, *Trans. Am. Nucl. Soc.*, **94**, pp 471-472, 2006.
- [28] J.W. Sterbentz, B. Phillips, R.L. Sant, G.S. Chang, & P.D. Bayless, “Reactor Physics Parametric and Depletion Studies in Support of TRISO Particle Fuel Specification for the Next Generation Nuclear Plant”, INEEL/EXT-04-02331, Idaho National Laboratory, September 2004.
- [29] J.W. Sterbentz, R.L. Sant, P.D. Bayless & R.R. Schultz, “NGNP Point Design—Results of the Initial Neutronics and Thermal-Hydraulic Assessments”, INEEL/EXT-03-00870, Idaho National Engineering and Environmental Laboratory, 2003.

Appendices

A Sample SCALE code for HTGR

```
=t-depl
HTR single-assembly model without burnable poison
44group
```

```
, _____
' — Materials _____
```

```
read comp
```

```
' — Fuel Kernel:
```

```
U-235 1 0 2.47519E-03 950 end
U-238 1 0 2.11461E-02 950 end
C 1 0 1.17950E-02 950 end
O-16 1 0 3.53850E-02 950 end
```

```
' — Buffer:
```

```
C-graphite 2 0 5.01791E-02 950 end
```

```
' — IPyC:
```

```
C-graphite 3 0 9.53403E-02 950 end
```

```
' — SiC:
```

```
Si 4 0 4.80726E-02 950 end
C 4 0 4.80726E-02 950 end
```

```
' — OPyC:
```

```
C-graphite 5 0 9.38349E-02 950 end
```

```
' — Compact:
```

```
C-graphite 6 0 6.01898E-02 950 end
```

```
' — Element:
```

C-graphite 70 0 8.73117E-02 950 end
C-graphite 71 0 8.73117E-02 950 end
C-graphite 72 0 8.73117E-02 950 end

' — Coolant:

He 8 0 4.81452E-04 950 end
He 18 0 4.81452E-04 950 end

' — Burnable poison:

B-10 21 0 1.58597E-04 950 end
B-11 21 0 1.60337E-05 950 end
C 21 0 6.24123E-02 950 end
B-10 22 0 1.58597E-04 950 end
B-11 22 0 1.60337E-05 950 end
C 22 0 6.24123E-02 950 end
B-10 23 0 1.58597E-04 950 end
B-11 23 0 1.60337E-05 950 end
C 23 0 6.24123E-02 950 end
B-10 24 0 1.58597E-04 950 end
B-11 24 0 1.60337E-05 950 end
C 24 0 6.24123E-02 950 end
B-10 25 0 1.58597E-04 950 end
B-11 25 0 1.60337E-05 950 end
C 25 0 6.24123E-02 950 end
B-10 26 0 1.58597E-04 950 end
B-11 26 0 1.60337E-05 950 end
C 26 0 6.24123E-02 950 end
B-10 27 0 1.58597E-04 950 end
B-11 27 0 1.60337E-05 950 end
C 27 0 6.24123E-02 950 end
B-10 28 0 1.58597E-04 950 end
B-11 28 0 1.60337E-05 950 end
C 28 0 6.24123E-02 950 end
B-10 29 0 1.58597E-04 950 end
B-11 29 0 1.60337E-05 950 end
C 29 0 6.24123E-02 950 end
B-10 30 0 1.58597E-04 950 end
B-11 30 0 1.60337E-05 950 end
C 30 0 6.24123E-02 950 end

' — Control rod:

B-10 10 0 1.05773E-02 950 end

B-11 10 0 1.06891E-03 950 end

C 10 0 1.47097E-02 950 end

end comp

'

' — Cell data

read celldata

doublehet fuelmix=100 end

gfr=0.017500 1

coatr=0.027500 2

coatr=0.031000 3

coatr=0.034500 4

coatr=0.038500 5

matrix=6

numpar=7256 end grain

rod triangpitch right_bdy=white left_bdy=reflected

hpitch=0.93980 71

fuelh=4.93

fuelr=0.62250

gapr=0.63500 8 end

end celldata

read depletion 1 end

end depletion

READ burndata

power=20.48 burn=545 nlib=1 end

END burndata

read model

44 group solution

```
, _____  
' — Parameters _____
```

```
read parm  
drawit=yes  
echo=yes  
prtxsec=1d  
prtmxsec=1d  
prtflux=yes  
prthmmix=no  
run=yes  
timed=yes  
epsilon=1e-6  
cmfd=no  
xycmfd=1  
end parm
```

```
read materials  
70 2 'graphite' end  
21 2 'poison' end  
22 2 'poison' end  
23 2 'poison' end  
24 2 'poison' end  
25 2 'poison' end  
26 2 'poison' end  
27 2 'poison' end  
28 2 'poison' end  
29 2 'poison' end  
30 2 'poison' end  
8 0 'coolant' end  
71 2 'graphite' end  
72 2 'graphite' end  
100 2 'fuel mix' end  
end materials
```

```
, _____  
' — Geometry _____
```

```
read geom
```

```
' — Compact:
```

unit 1

cylinder 1 0.62250
cylinder 2 0.63500
hexprism 3 0.93980

media 100 1 1
media 8 1 2 -1
media 71 1 3 -2

boundary 3 5 5

' — Burnable poison:

unit 2

cylinder 1 0.06225
cylinder 2 0.1245
cylinder 3 0.18675
cylinder 4 0.249
cylinder 5 0.31125
cylinder 6 0.3735
cylinder 7 0.43575
cylinder 8 0.498
cylinder 9 0.56025
cylinder 10 0.6225
cylinder 11 0.63500
hexprism 12 0.93980

media 21 1 1
media 22 1 2 -1
media 23 1 3 -2
media 24 1 4 -3
media 25 1 5 -4
media 26 1 6 -5
media 27 1 7 -6
media 28 1 8 -7
media 29 1 9 -8
media 30 1 10 -9
media 8 1 11 -10
media 72 1 12 -11

boundary 12 10 10

' — Coolant hole:

unit 3

cylinder 1 0.79375
hexprism 2 0.93980

media 8 1 1
media 70 1 2 -1

boundary 2 5 5

' — Inner coolant hole:

unit 4

cylinder 1 0.63500
hexprism 2 0.93980

media 8 1 1
media 70 1 2 -1

boundary 2 5 5

' — Empty lattice position:

unit 5

hexprism 1 0.93980

media 70 1 1

boundary 1

' — Lattice:

unit 99

rhexprism 1 17.99844
rhexprism 2 18.0
array 20 1 place 12 12 0.0 0.0
media 70 1 1
media 8 1 2 -1

```

boundary 2

global unit 100
hole 99
hole 99 origin x=31.2140 y=18.00
cuboid 1 31.2140 0.0 18.00 0.0
media 70 1 1
boundary 1 31 18
end geom

read array

ara=20 nux=23 nuy=23 typ=hexagonal
fill
00000000000000000000000000000000
0000000000000213113113113120
0000000000001311311311311310
0000000000031131131131131130
0000000000113113113113113110
0000000013113113113113113110
000000031131131131131131130
000000113113113113113113110
000001311311311311311311310
00031131131141131131131130
00113113114004113113113110
02311311310501311311311320
01131131140041131131131100
03113113114113113113113000
01311311311311311311310000
01131131131131131131100000
03113113113113113113000000
01311311311311311310000000
01131131131131131100000000
03113113113113113000000000
01311311311311310000000000
021311311312000000000000
00000000000000000000000000 end fill

end array
, _____

end model

```

```
end
=shell
open $RTNDIR/htgr_depl.newtmatl.ps
end
```

B Power Peaking by Fuel Rod

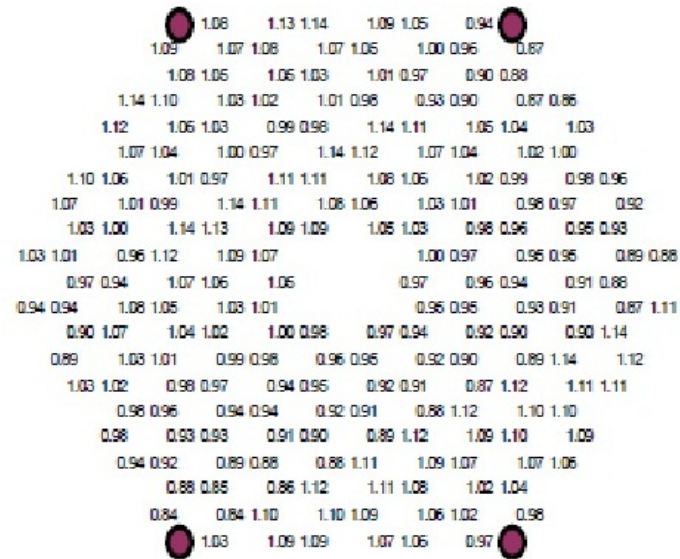


Figure 24: Used to determine power density in the 6th ring of the core[28].

C Illustration of NEWT

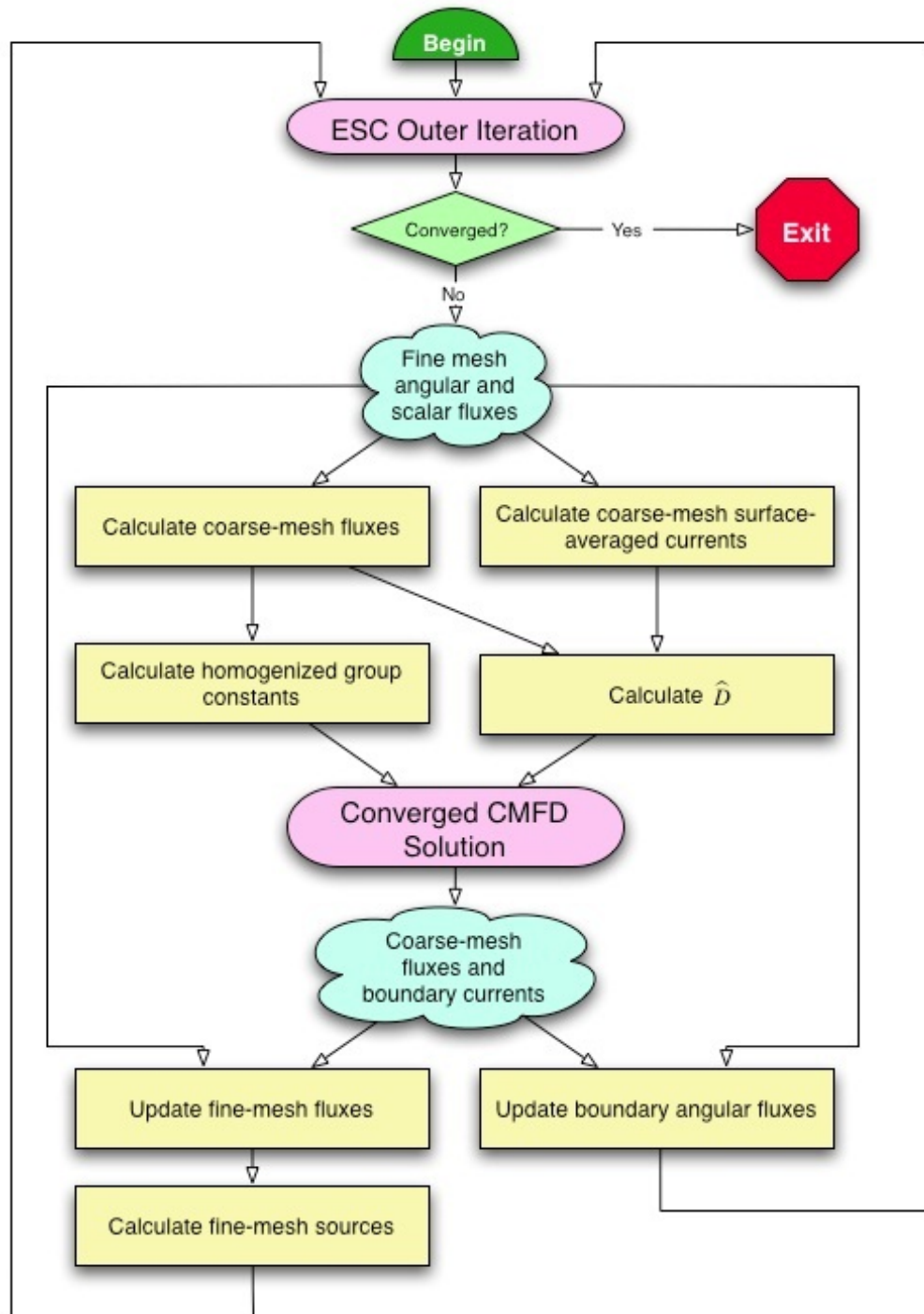


Figure 27: An illustration of how NEWT solves a transport problem[24].